

1 **Seasonal cycles of biogeochemical fluxes in the Scotia Sea, Southern Ocean: A stable isotope**  
2 **approach**

3

4 Anna Belcher<sup>1</sup>, Sian F. Henley<sup>2</sup>, Katharine Hendry<sup>1,3</sup>, Marianne Wootton<sup>4</sup>, Lisa Friberg<sup>3</sup>, Ursula  
5 Dallman<sup>2</sup>, Tong Wang<sup>3</sup>, Christopher Coath<sup>3</sup>, Clara Manno<sup>1</sup>

6 <sup>1</sup> British Antarctic Survey, Cambridge, CB3 0ET, UK

7 <sup>2</sup> School of Geosciences, University of Edinburgh, Edinburgh EH9 3FE, UK

8 <sup>3</sup> University of Bristol, Bristol, BS8 1RJ, UK

9 <sup>4</sup> Marine Biological Association, Plymouth, PL1 2PB, UK

10

11 Correspondence to: Anna Belcher ([annbel@bas.ac.uk](mailto:annbel@bas.ac.uk)) and Clara Manno ([clanno@bas.ac.uk](mailto:clanno@bas.ac.uk))

12

13 **Abstract**

14 The biological carbon pump is responsible for much of the decadal variability in the ocean carbon  
15 dioxide (CO<sub>2</sub>) sink, driving the transfer of carbon from the atmosphere to the deep ocean. A  
16 mechanistic understanding of the ecological drivers of particulate organic carbon (POC) flux is key to  
17 both the assessment of the magnitude of the ocean CO<sub>2</sub> sink, as well as for accurate predictions as to  
18 how this will change with changing climate. This is particularly important in the Southern Ocean, a  
19 key region for the uptake of CO<sub>2</sub> and the supply of nutrients to the global thermocline. In this study  
20 we examine sediment trap derived particle fluxes and stable isotope signatures of carbon (C),  
21 nitrogen (N) and biogenic silica (BSi) at a study site in the biologically productive waters of the  
22 northern Scotia Sea in the Southern Ocean. Both deep (2000 m) and shallow (400 m) sediment traps  
23 exhibited two main peaks in POC, particulate nitrogen and BSi flux, one in austral spring and one in  
24 summer, reflecting periods of high surface productivity. Particulate fluxes and isotopic compositions  
25 were similar in both deep and shallow sediment traps, highlighting that most remineralisation  
26 occurred in the upper 400 m of the water column. Differences in the seasonal cycles of isotopic  
27 compositions of C, N and Si provide insights into the degree of coupling of these key nutrients. We  
28 measured increasing isotopic enrichment of POC and BSi in spring, consistent with fractionation  
29 during biological uptake. Since we observed isotopically light particulate material in the traps in  
30 summer, we suggest physically-mediated replenishment of lighter isotopes of key nutrients from  
31 depth, enabling full expression of the isotopic fractionation associated with biological uptake. The  
32 change in the nutrient and remineralisation regimes, indicated by the different isotopic  
33 compositions of the spring and summer productive periods, suggests a change in the source region  
34 of material reaching the traps and associated shifts in phytoplankton community structure. This,  
35 combined with the occurrence of advective inputs at certain times of the year, highlights the need to  
36 make synchronous measurements of physical processes to improve our ability to track changes in  
37 the source regions of sinking particulate material. We also highlight the need to conduct particle-  
38 specific (e.g. faecal pellet, phytoplankton detritus, zooplankton moults) isotopic analysis to improve

39 the use of this tool in assessing particle composition of the sinking material and develop our  
40 understanding of the drivers of biogeochemical fluxes.

41

## 42 **1. Introduction**

43 The transfer of carbon from the atmosphere to the deep ocean via the biological carbon pump (Volk  
44 and Hoffert, 1985) is important for the sequestration of carbon, and combined with ocean  
45 circulation is a main driver of decadal variability of the ocean carbon dioxide (CO<sub>2</sub>) sink (DeVries,  
46 2022). Mechanistic understanding of the processes controlling the magnitude and efficiency of the  
47 biological carbon pump is therefore key to assessment and prediction of the ocean's role as a CO<sub>2</sub>  
48 sink and requires robust characterisation of the composition of the sinking particles transferring  
49 particulate organic carbon (POC) to the deep ocean. The composition of particles affects the sinking  
50 rate, lability and thus degree of remineralisation as they sink through the water column (e.g. Ploug  
51 et al., 2008; Giering et al., 2020).

52 Sediment traps enable visual assessment of sinking particles, and have been deployed in numerous  
53 locations throughout the world's oceans to both quantify biogeochemical fluxes and characterise the  
54 nature of sinking material (for example data compilation of Atlantic Ocean sediment traps; Torres  
55 Valdés et al., 2014). Sediment traps can be susceptible to collection biases depending on the depth  
56 of deployment, trap design, hydrodynamic conditions and properties of sinking particles (Buesseler  
57 et al., 2007). Moored sediment traps can underestimate the actual flux at depths shallower than  
58 ~1500 m by collecting only a portion of the sinking material, though biases vary greatly between  
59 sites (Buesseler et al., 2007). Numerous studies have recorded the dominance of particular  
60 organisms or types of detrital material in trap material, highlighting the importance of ecosystem  
61 community structure on the magnitude and efficiency of the biological carbon pump. For example,  
62 faecal pellets, diatoms, diatom resting spores and acantharia have been observed as significant  
63 contributors to particle fluxes (González et al., 2009; Belcher et al., 2018, 2017; Manno et al., 2015;  
64 Gleiber et al., 2012; Rembauville et al., 2015; Roca-Marti et al., 2017). Such visual assessment of trap  
65 material is typically very time consuming. Additionally, fragile material, such as salp faecal pellets  
66 (Iversen et al., 2017; Pauli et al., 2021) may break up in the sample manipulation processes, making  
67 them hard to account for visually. Biogeochemical methods such as the use of stable isotopes may  
68 offer additional insight into the drivers of POC fluxes (e.g. Henley et al., 2012).

69 Marine phytoplankton take up aqueous CO<sub>2</sub> ([CO<sub>2(aq)</sub>]) during photosynthesis, converting it to organic  
70 carbon. During this process, the lighter isotope (<sup>12</sup>C) is preferentially assimilated, which enriches the  
71 residual aqueous pool in the heavier isotope (<sup>13</sup>C). The stable isotopic composition of the POC  
72 ( $\delta^{13}\text{C}_{\text{POC}}$ ) of the marine phytoplankton is therefore lower than that of the carbon source. Over large  
73 scales, the  $\delta^{13}\text{C}$  of marine phytoplankton has been found to be inversely correlated with [CO<sub>2(aq)</sub>] in  
74 surface waters (Rau et al., 1991). However, numerous other factors have been identified as  
75 impacting the  $\delta^{13}\text{C}_{\text{POC}}$  of surface waters and marine plankton. Phytoplankton growth rates, cell  
76 geometry and non-diffusive uptake of carbon via carbon concentration mechanisms have all been  
77 highlighted as impacting the  $\delta^{13}\text{C}_{\text{POC}}$  of marine plankton and thus surface waters (Popp et al., 1999,  
78 1998; Bidigare et al., 1999; Trull and Armand, 2001; Tuerena et al., 2019). This decoupling of the  
79 relationship between  $\delta^{13}\text{C}_{\text{POC}}$  and [CO<sub>2(aq)</sub>] presents challenges for palaeoceanographic studies, but

80 also the possibility of using the  $\delta^{13}\text{C}_{\text{POC}}$  of marine samples to infer information about community  
81 composition.

82 During photosynthetic uptake, the balance between supply and demand of carbon impacts  $\delta^{13}\text{C}_{\text{POC}}$ ,  
83 regulated by the transport into the internal cell and fixation to organic carbon (Popp et al., 1999;  
84 Trull and Armand, 2001). A greater isotopic fractionation occurs in smaller phytoplankton cells,  
85 enabled by the higher cell surface area to volume (SA:V) ratios and increased amount of  $[\text{CO}_{2(aq)}]$   
86 diffusing across the cell membrane relative to the total carbon within the cell (Popp et al., 1998;  
87 Tuerena et al., 2019; Hansman and Sessions, 2016). Thus, a community dominated by large, fast-  
88 growing diatoms is expected to contribute to enriched  $\delta^{13}\text{C}_{\text{POC}}$  values compared to a community  
89 dominated by picoplankton. A study by Henley et al. (2012) in the coastal western Antarctic  
90 Peninsula, attributed a large (~10 ‰) negative isotopic shift in  $\delta^{13}\text{C}_{\text{POC}}$  to a near-complete biomass  
91 dominance of the marine diatom *Proboscia inermis* highlighting the possible impact of shifts in  
92 species composition on stable isotopes. It may therefore be possible to use stable isotopes to gain  
93 information about the community composition of phytoplankton driving, for example, large spring  
94 pulses in POC flux. Additionally, siliceous phytoplankton, such as diatoms, require dissolved silica  
95 (silicic acid, or DSi) to build their cell walls or frustules (amorphous  $\text{SiO}_2 \cdot n\text{H}_2\text{O}$ , referred to here as  
96 biogenic silica, BSi). During uptake of DSi, diatoms fractionate the stable isotopes of silicon ( $^{28}\text{Si}$ ,  $^{29}\text{Si}$ ,  
97  $^{30}\text{Si}$ ) preferentially taking up the lighter isotopes during cell wall (frustule) formation (De La Rocha et  
98 al., 1997). This means that BSi fluxes and ratios of light  $^{28}\text{Si}$  to heavy  $^{30}\text{Si}$  (expressed as  $\delta^{30}\text{Si}$ ) in  
99 sinking particulate organic matter (POM) can be informative about DSi utilisation by siliceous  
100 phytoplankton. The fractionation of Si isotopes during diatom DSi utilisation is approximately -1.1  
101 ‰, although estimates of this value vary in laboratory and field studies between -0.5 and -2.5 ‰  
102 (Hendry and Brzezinski, 2014). Whilst some studies have shown that isotopic fractionation is  
103 independent of temperature, DSi and diatom species (e.g., De La Rocha et al., 1997), one *in vitro*  
104 laboratory culture experiment revealed a potential species effect, with polar species exhibiting more  
105 extreme fractionation (-2.09 ‰ for *Chaetoceros* sp. and 0.54 ‰ *Fragilariopsis kerguelensis*, Sutton et  
106 al., 2013). The impact of water column dissolution on frustule  $\delta^{30}\text{Si}$  is poorly constrained, with  
107 experimental evidence for either a small fractionation of -0.55 ‰ (Demarest et al., 2009) or a  
108 negligible impact (Wetzel et al., 2014; Egan et al., 2012; Grasse et al., 2021).

109 Additionally, the stable isotopes of marine nitrogen reveal information about uptake of inorganic  
110 nitrogen sources by phytoplankton (Wada and Hattori, 1978), as well as trophic and food web  
111 processes (Michener and Lajtha, 2008). Nitrogen has two isotopes,  $^{14}\text{N}$ , and  $^{15}\text{N}$ , and the ratio  
112 between these heavy and light isotopes is expressed as  $\delta^{15}\text{N}$ . Different sources of nitrogen can alter  
113 the stable isotopic composition of marine phytoplankton because ammonium characteristically has a  
114 lower value of  $\delta^{15}\text{N}$  than nitrate supplied from depth. As well as this, isotopic fractionation occurs  
115 during transfer through the food web, with a trophic enrichment of typically 2-4 ‰ between  
116 successive trophic levels (Montoya, 2007; Minagawa and Wada, 1984). Excretion and egestion  
117 processes can impact  $\delta^{15}\text{N}$ ; isotopic discrimination during excretion of ammonium by zooplankton  
118 and fish results in ammonium that is  $^{15}\text{N}$ -depleted relative to the substrate catabolised (Montoya,  
119 2007). Thus, there are several interacting processes impacting the degree of fractionation and  
120 subsequent isotopic ratios in particulate nitrogen (PN) and knowledge of  $\delta^{15}\text{N}$  ratios may provide  
121 insight into biogeochemical processes and the composition of the sinking flux.

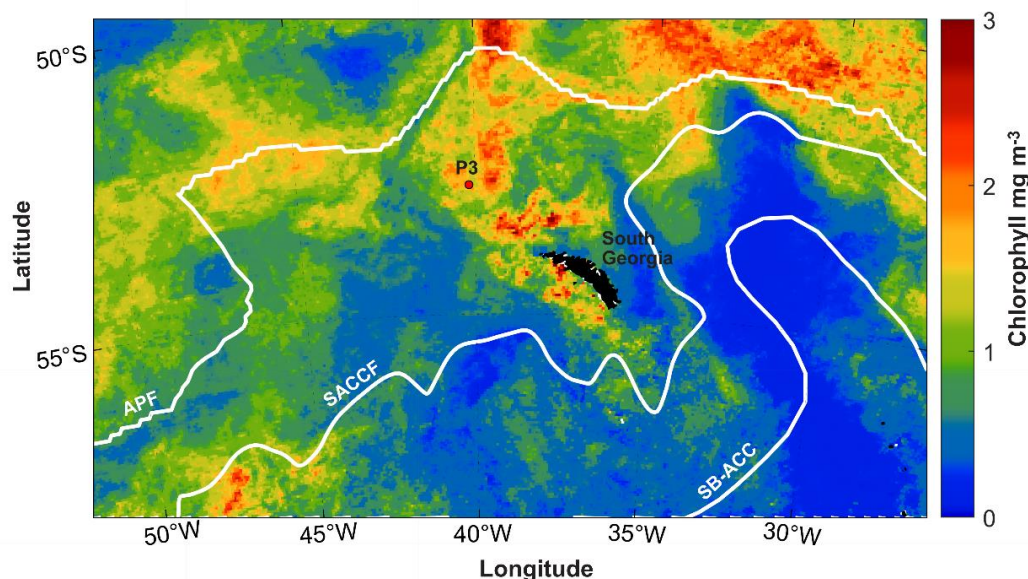
122 In this study we examine the seasonal cycle of the magnitude and composition of vertical  
123 biogeochemical fluxes of particulate material collected by two sediment traps deployed for almost  
124 one year on a deep ocean mooring located in the northern Scotia Sea in the Atlantic sector of the  
125 Southern Ocean. The Scotia Sea, particularly the region downstream of South Georgia is a hot spot  
126 for biological productivity, supported by higher iron availability (Korb et al., 2008; Matano et al.,  
127 2020). Diatoms dominate the phytoplankton assemblage, particularly in the summer months, with  
128 smaller contributions of dinoflagellates (Korb et al., 2012). The large, consistent phytoplankton  
129 blooms occurring in this region support high fluxes of POC to the deep ocean, with two peaks in POC  
130 flux occurring during the seasonal cycle; first peak in austral spring, and second in late summer or  
131 early autumn (Manno et al., 2015). Faecal pellets (up to 91 % in late spring and early summer,  
132 Manno et al., 2015), krill exuviae (up to 47 % in summer, Manno et al., 2020) and diatoms,  
133 particularly resting spores (annual contribution of 42 %, Rembauville et al., 2016) have been shown  
134 to make large contributions to the POC fluxes in our study region. Here we use  $\delta^{13}\text{C}_{\text{POC}}$ ,  $\delta^{15}\text{N}_{\text{PN}}$  and  
135  $\delta^{30}\text{Si}_{\text{BSi}}$  alongside calculated fluxes of POC, PN and BSi as tools to reveal information about sinking  
136 particulate organic matter and the processes influencing its production and subsequent flux to  
137 depth. More in-depth understanding of the composition, and thus the drivers of POC flux in this  
138 important region are key to improving estimates of the current and future strength of the biological  
139 carbon pump and the ocean's role as a  $\text{CO}_2$  sink.

140

## 141 2. Methods

### 142 2.1. Study Area

143 This study was conducted in the open ocean environment of the northern Scotia Sea in the Southern  
144 Ocean at a long-term observatory station, P3 (Figure 1), where an oceanographic mooring is located.  
145 The mooring is part of the Scotia Sea Open Ocean Observatory (SCOOBIES:  
146 <https://www.bas.ac.uk/project/scoobies/>), a programme designed to investigate the biological and  
147 biogeochemical influence of the large and persistent phytoplankton bloom to the northwest of  
148 South Georgia.



149

150 **Figure 1: Location of P3 mooring site to the northwest of South Georgia. White lines indicate**  
151 **frontal positions of the Antarctic Polar Front (APF) (Moore et al., 1999), Southern Antarctic**  
152 **Circumpolar Current Front (SACCF) (Thorpe et al., 2002) and the Southern Boundary of the**  
153 **Antarctic Circumpolar Current (SB-ACC) (Orsi et al., 1995). Mean chlorophyll concentration ( $\text{mg m}^{-3}$ )**  
154 **is shown for December 2018 from 8-day satellite chlorophyll data from the Ocean Colour CCI**  
155 **(version 5.0) (Sathyendranath et al., 2021, 2019).**

156

## 157 2.2. Sediment trap deployment

158 Two sediment traps were deployed on the mooring array to collect sinking particles for analysis of  
159 carbon, nitrogen and biogenic silica fluxes and analysis of  $\delta^{13}\text{C}_{\text{POC}}$ ,  $\delta^{15}\text{N}_{\text{PN}}$  and  $\delta^{30}\text{Si}_{\text{BSi}}$ . The mooring  
160 was deployed from 25<sup>th</sup> January 2018, during research cruise JR17002 aboard the *RRS James Clark*  
161 *Ross*, to 1<sup>st</sup> January 2019, recovered during research cruise DY098 aboard the *RRS Discovery*. The  
162 mooring was located at 52.8036 °S, 40.1593 °W, to the northwest of South Georgia island in the  
163 Scotia Sea at a water depth of 3748 m. Sediment traps (McLane PARFLUX, 0.5 m<sup>2</sup> surface collecting  
164 area; McLane labs, Falmouth, MA, USA) were deployed at 400 and 2000 m (referred herein as  
165 shallow and deep respectively) and were each equipped with 21 sample bottles. A baffle at the top  
166 of the trap prevents large organisms from entering and each sample bottle contained a formosaline  
167 solution (filtered seawater containing 2 % v/v formalin, mixed with sodium tetraborate (BORAX;  
168 0.025 % w/v), and 0.5 % w/v sodium chloride) to prevent mixing with the overlying water column  
169 and stop biological degradation. Previous studies have reported the effects of formalin on  $\delta^{13}\text{C}_{\text{POC}}$   
170 and  $\delta^{15}\text{N}_{\text{PN}}$  to be small ( $\pm 1$  ‰ and  $\pm 1.5$  ‰ respectively, Mincks et al., 2008 and references therein).  
171 This equates to 13 % and 16 % of the maximum range measured in our study, which is small  
172 compared to the isotopic shifts we observed. Yet we stress that all  $\delta^{13}\text{C}_{\text{POC}}$  and  $\delta^{15}\text{N}_{\text{PN}}$  values given  
173 here are associated with this uncertainty. The sediment trap sample carousel was programmed to  
174 rotate every 7-31 days depending on the season; shorter periods to coincide with austral summer  
175 and longer periods during austral winter (Table S1). TM Seaguard current meters were deployed ~50  
176 m above the shallow sediment trap and 50 m below the deep sediment trap, set at a measurement  
177 interval of 2 hours.

## 178 2.3. Trap sample processing

179 Each sample bottle from the sediment trap was processed on return to the laboratory. The  
180 supernatant was carefully removed using a syringe and swimmers (zooplankton that are believed to  
181 have entered the trap actively whilst alive) were removed. Swimmers were removed by hand under  
182 a dissecting microscope and were not included in flux calculations. The material from each sediment  
183 trap sample bottle was split into a number of smaller aliquots for subsequent analysis using a  
184 McLane rotary splitter.

185

### 186 2.3.1. Organic carbon and nitrogen

187 For each sediment trap bottle from both deep and shallow traps, two or three splits were taken and  
188 each analysed for POC and PN mass and  $\delta^{13}\text{C}_{\text{POC}}$  and  $\delta^{15}\text{N}_{\text{PN}}$ . Once split, the material was filtered onto  
189 pre-combusted (450 °C, 16h) 25 mm glass fibre filters (GF/F; nominal pore size 0.7  $\mu\text{m}$ ) and rinsed  
190 with milli-Q water. Samples were air dried, fumed for 24 h with 37 % HCl in a desiccator, before

191 finally oven-drying at 50 °C for 24 h. Filters and filter blanks were placed in sterile tin capsules and  
192 POC and PN measured on a CE Instruments NA2500 Elemental analyser, calibrated using an  
193 acetanilide calibration standard with a known %C and %N of 71.09 % and 10.36 % respectively.  
194 Standards were interspersed regularly between samples to measure and correct for drift. Analytical  
195 precision was better than 1.0 % for POC and 1.1 % for PN. The POC flux ( $F, mg C m^{-2} d^{-1}$ ) for each  
196 sample was calculated using the following equation:

$$197 \quad F = m / (A \times d) \quad (1)$$

198 Here  $m$  is the mass of POC in the sample bottle (mg),  $d$  is the number of days that the sample bottle  
199 was open (7–31 days) and  $A$  is the surface area of the sediment trap opening ( $0.5 m^2$ ). The same  
200 calculation was carried out for PN.

201  $\delta^{13}C_{POC}$  and  $\delta^{15}N_{PN}$  were analysed on a Thermo Finnigan Delta-Plus Advantage isotope ratio mass  
202 spectrometer that was in line with the elemental analyser. All  $\delta^{13}C_{POC}$  and  $\delta^{15}N_{PN}$  data are presented  
203 in the delta per mille (‰) notation relative to the appropriate international standard, according to  
204 equation 2.

$$205 \quad \delta X (\text{‰}) = 10^3 (R_{sample} / R_{standard} - 1) \quad (2)$$

206  $R$  denotes the  $^{13}C/^{12}C$  ratio for carbon or the  $^{15}N/^{14}N$  ratio for nitrogen.  $R_{sample}$  refers to the relevant  
207 ratio in the sample.  $R_{standard}$  refers to the ratios in the international standards Vienna Pee Dee  
208 belemnite (V-PDB for  $\delta^{13}C$  and atmospheric nitrogen (AIR) for  $\delta^{15}N$ ), both of which are calibrated  
209 against the PACS-2 marine sediment reference material. Multiple repeats of analytical standards  
210 gives a reproducibility of 0.2 ‰ for C and N, which is significantly smaller than the uncertainty  
211 associated with organic carbon in the formalin preservative ( $\pm 1 \text{‰}$  and  $\pm 1.5 \text{‰}$  for C and N  
212 respectively, Mincks et al., 2008 and references therein).

213

### 214 *2.3.2. Biogenic silica*

215 Two splits were taken from each sample bottle from both deep and shallow sediment traps for  
216 analysis of biogenic silica and silicon isotopes. Split material was filtered onto 25 mm,  $0.4 \mu m$ ,  
217 polycarbonate filters and rinsed with Milli-Q water before drying at 50 °C for 24h. Material on the  
218 filters was solubilised via an alkaline extraction method (Hatton et al., 2019) carried out at the Bristol  
219 Isotope Group (BIG) laboratory. Sample material was digested in Teflon tubes with 0.2M NaOH at  
220 100 °C for 40 minutes. This was followed by neutralisation with 6M HCl. Biogenic silica ( $SiO_2$ , termed  
221 BSi) concentrations were measured chlorometrically by molybdate blue spectrophotometry  
222 (Heteropoly Blue Method) (Strickland and Parsons, 1972) using a Hach DR3900 spectrophotometer  
223 set at a wavelength of 815 nm. Supernatants were stored for 7-11 months before column chemistry  
224 for isotope analysis. Fluxes of biogenic silica were calculated as for POC using equation 1.

225 For Si isotope analysis, supernatants and reference materials were purified by passing through  
226 cation exchange columns (Bio-Rad AG50W-X12, 200-400 mesh resin) pre-cleaned with HCl following  
227 Georg et al. (2006). Samples were acidified to a pH of 1-2 to ensure that all the silicon remained in  
228 solution. Samples were loaded onto columns and eluted with Milli-Q water to produce a 2.5 ppm  
229 solution, and concentrations were checked to confirm quantitative yields. Si isotopic composition  
230 was analysed within 24 hours of column chemistry. Stable Si isotopic compositions were measured

231 at the BIG laboratory on a Finnigan Neptune Plus High-Resolution MC-ICP-MS (Thermo Fisher  
232 Scientific). The Si solutions were spiked with magnesium spike (Inorganic Ventures MSMG-10 ppm),  
233 hydrochloric acid (1M HCl in-house distilled) and sulphuric acid (0.1M H<sub>2</sub>SO<sub>4</sub>, ROMIL-UpA™ Ultra  
234 Purity Sulphuric Acid), and transferred from the autosampler via a PFA Savillex C-Flow nebulizer (35  
235 μl min<sup>-1</sup>) connected to an Apex IR Desolvating Nebulizer (Ward et al., 2022), and measured on the  
236 low-mass side to resolve any isobaric interferences (e.g., <sup>14</sup>N<sup>16</sup>O<sup>+</sup>). All standards and samples were  
237 blank-corrected offline. The intensity of <sup>28</sup>Si in the 0.1M HCl blank was <1 % of the sample intensity  
238 in all sample runs. Furthermore, we also measured Mg isotopes (<sup>24</sup>Mg, <sup>25</sup>Mg and <sup>26</sup>Mg) as an internal  
239 isotopic reference to correct for any mass-dependent fractionation (White et al., 2000).  
240 Measurements that resulted in large corrections (>0.3 ‰ on δ<sup>30</sup>Si) underwent repeat analysis.  
241 Instrumental mass bias was further accounted for using a standard-sample bracketing method using  
242 a 2 ppm reference standard (NBS or RM8546) solution. Two splits were analysed for each sediment  
243 trap bottle, as well as standards and sample blanks. Solutions obtained from each split were  
244 measured in replicate (n = 2-3) alongside continuous measurement of reference materials Diatomite  
245 and LMG-08 to ensure reproducibility and to monitor data quality. Measurements of Diatomite and  
246 LMG-08 yielded δ<sup>30</sup>Si of +1.23 ‰ (SD ± 0.03, n=18) and -3.40 ‰ (SD ± 0.05, n=5) respectively, which  
247 agreed with published values (Reynolds et al., 2007; Hendry and Robinson, 2012; Grasse et al.,  
248 2017). Typical reproducibility between the sediment trap sample splits (coming from the same  
249 sediment trap bottle) was 0.034 ‰ (1 x SD). A lithogenic correction (e.g., Closset et al., 2015) was not  
250 carried out on these samples. However, even an extreme scenario of variable lithogenic  
251 contamination of 1-5 % of isotopically light marine clays (with δ<sup>30</sup>Si of -2.3 ‰; Opfergelt and  
252 Delmelle, 2012) would only result in a potential systematic offset of 0.12 ‰, which is an order of  
253 magnitude smaller than the observed seasonal signal.

#### 254 *Chlorophyll and phytoplankton community composition*

255 Surface chlorophyll concentrations were obtained from satellite-derived 8-day Ocean Colour CCI  
256 (version 5.0) (Sathyendranath et al., 2021, 2019). We present the monthly mean of these 8-day data  
257 for December at our study site (Figure 1), as well as the 8-day chlorophyll concentration data from  
258 September 2017 to December 2018 (Figure 2) averaged over a 1 x 1° bounding box around our study  
259 site (41 °W, 40 °W, 53 °S, 52 °S).

260 Light microscopy was used to assess phytoplankton and microzooplankton community composition  
261 of a small selection of samples from the two main productive periods. A biological method of sample  
262 preparation and analysis was chosen, comparable with Rembauville et al. (2015), to determine the  
263 quantity of empty and full cells. Following subsampling using the rotary splitter, samples for  
264 morphological taxonomic analysis were diluted to a standardised 25 ml. Samples were gently  
265 inverted using the Paul Schatz principle (figures of eight) for one minute to homogenise them, and 2  
266 ml was withdrawn using a modified pipette with widened opening. Several common diatoms in  
267 Antarctic waters are long and slim; in particular, *Thalassiothrix antarctica* has been recorded with an  
268 apical axis up to 5mm. To ensure such specimens remain intact and are not excluded from the  
269 pipetting process, a wide bore opening is necessary. The 2 ml subsamples were used to fill a 1 ml  
270 Sedgwick Rafter counting chamber. Chambers were viewed using a compound light microscope  
271 (Nikon Eclipse 80i) with differential interference contrast at x200 magnification. For the larger, easily  
272 identifiable cells, the whole chamber was observed; for smaller cells a proportion of the chamber  
273 was examined depending upon cell abundance (at least 500 cells were counted). Only complete cells

274 were enumerated to avoid over counting of fragmented specimens. Cells were determined as “full”  
275 or alive at time of collection if they possessed chloroplasts/plastids, pigment, a nucleus or, in the  
276 case of *Pronoctiluca*, a distinct accumulation body; cells lacking these internal features were deemed  
277 as “empty”, or dead at time of collection. Specimens were identified according to Hasle and  
278 Syvertsen (1997); Medlin and Priddle (1990); Priddle and Fryxell (1985) and Scott and Marchan  
279 (2005).

280 Cell bio-volume and surface area estimates were calculated using geometrics and the appropriate  
281 shape-related equations for phytoplankton genera proposed by Hillebrand et al. (1999). Metrics  
282 used in the calculations were based on the average size of ten randomly selected specimens  
283 belonging to a species/taxonomic group within the samples.

284

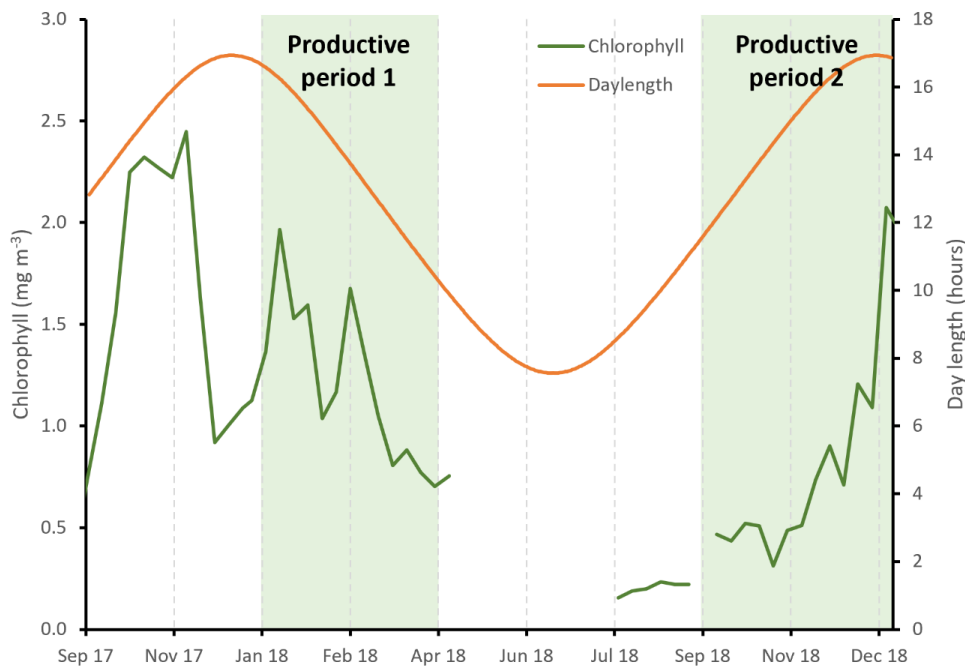
### 285 3. Results

#### 286 3.1. Environmental conditions

287 Mean current velocities were  $0.11 (\pm 0.06)$  and  $0.06 (\pm 0.03)$   $\text{m s}^{-1}$  for shallow and deep current  
288 meters respectively (Supplementary Figure S1). Maximum current speeds recorded reached  $0.43$   
289 and  $0.18$   $\text{m s}^{-1}$  for shallow and deep meters respectively. The periods with currents substantially  
290 elevated above the mean were June for both traps, and additionally in late August/September for  
291 the shallow trap, both for periods of ~5-10 days. Both are periods of low fluxes during austral winter  
292 and are not the main subject of the study here, though it is likely that particle collection was biased  
293 at these times (Buesseler et al., 2007).

294 Satellite-derived estimates of surface chlorophyll show high concentrations during austral summer  
295 (January to March) peaking at  $2.3 \text{ mg m}^{-3}$ , as well as during spring (November-December), peaking at  
296  $2.1 \text{ mg m}^{-3}$  (Figure 2, Figure S2). Data coverage is limited in the winter due to cloud cover, but  
297 concentrations appear to be  $<0.4 \text{ mg m}^{-3}$ . We define here two productive periods (when chlorophyll  
298 concentrations were  $>0.4 \text{ mg m}^{-3}$ ), which we refer to throughout the manuscript, productive period  
299 1: January to April 2018, and productive period 2: September to December 2018. We note that our  
300 sediment trap data begins on the 25<sup>th</sup> January so we do not capture the start of period 1.





301 **Figure 2:**  
 302 **Seasonal cycle of satellite derived surface chlorophyll concentration (green line, 8-day data from**  
 303 **the Ocean Colour CCI (version 5.0) (Sathyendranath et al., 2021, 2019)). Daylength at 53 °S is shown**  
 304 **by the orange line. The two productive periods are highlighted by the shaded green region.**

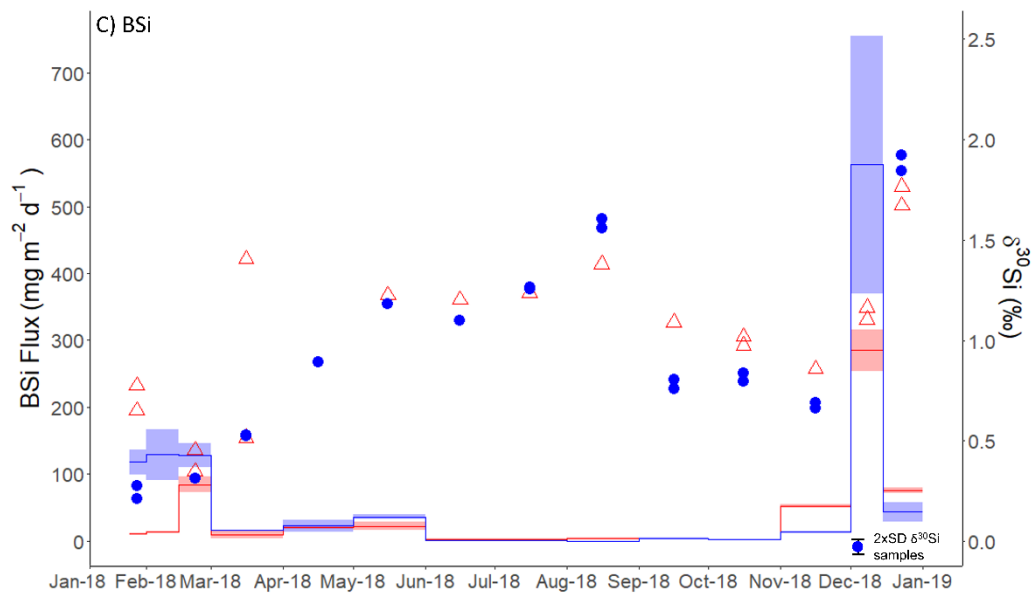
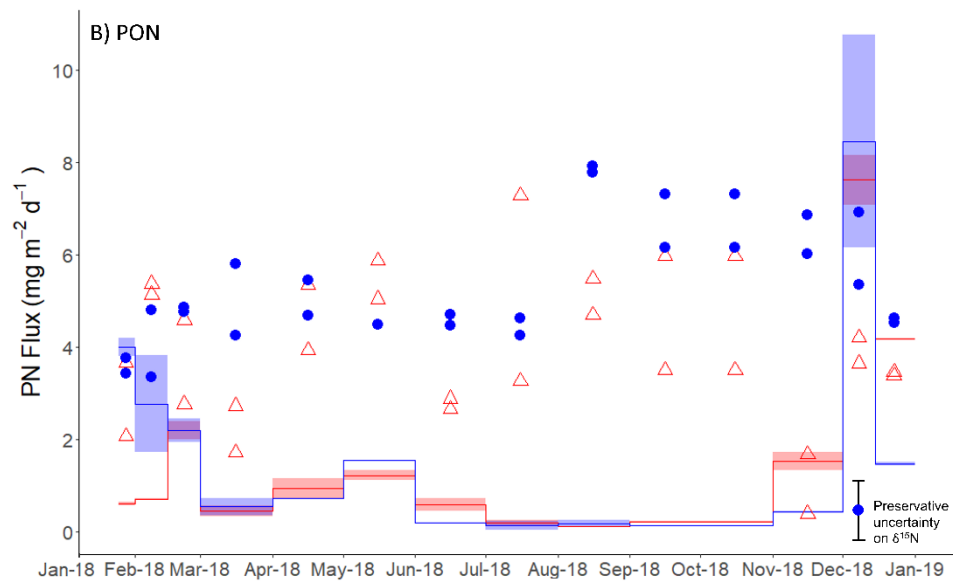
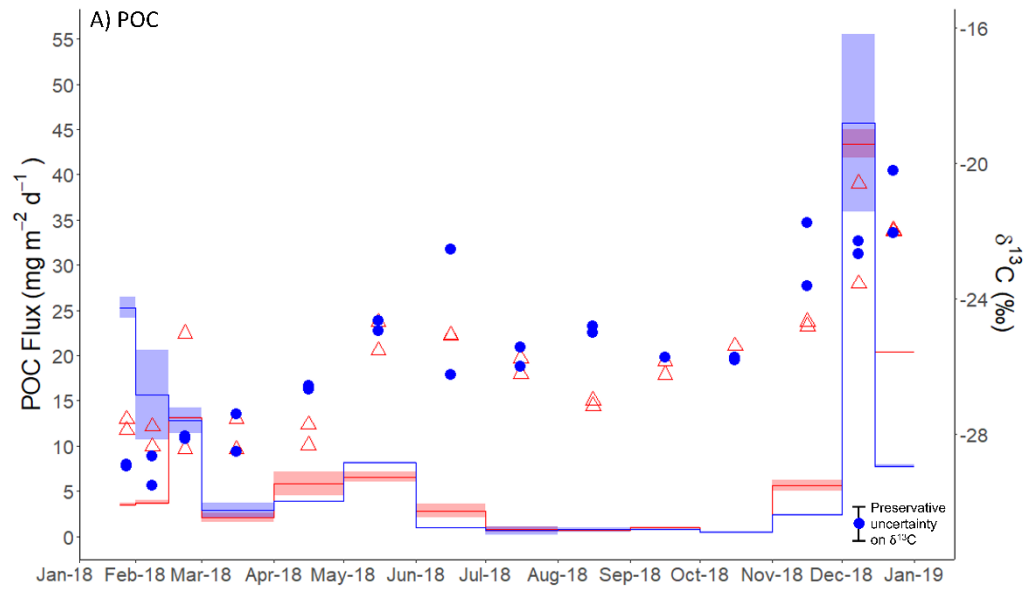
305

306 3.2. POC, PN, BSi fluxes

307 There is a clear seasonal cycle in POC, PN and BSi fluxes, all tracking each other well (Figure 3). Since  
 308 two to three splits were analysed from each sediment trap bottle, we refer here to the mean flux for  
 309 each sediment trap bottle based on the available splits for that bottle. POC fluxes were low during  
 310 austral autumn and winter, with fluxes  $<10 \text{ mg C m}^{-2} \text{ d}^{-1}$  and  $<7 \text{ mg C m}^{-2} \text{ d}^{-1}$  for shallow and deep  
 311 traps respectively during the period March to October 2018. Higher fluxes were measured in  
 312 summer 2018 (productive period 1), reaching  $25.3 \text{ mg C m}^{-2} \text{ d}^{-1}$  in late January 2018 in the shallow  
 313 trap and  $13.1 \text{ mg C m}^{-2} \text{ d}^{-1}$  in late February in the deep trap. The maximum POC fluxes measured  
 314 occurred in early December 2018 (productive period 2), reaching  $45.7 \text{ mg C m}^{-2} \text{ d}^{-1}$  and  $43.4 \text{ mg C m}^{-2}$   
 315  $\text{d}^{-1}$ , in shallow and deep traps respectively. PN fluxes follow the same trends as POC fluxes, peaking  
 316 at  $4.2$  and  $2.4 \text{ mg N m}^{-2} \text{ d}^{-1}$  during period 1, and  $10.8$  and  $8.2 \text{ mg N m}^{-2} \text{ d}^{-1}$  during period 2, in shallow  
 317 and deep traps respectively (Figure 3B). The mean POC:PN ratio (mol:mol) throughout the study  
 318 period was  $6.40 (\pm 0.73)$  and  $6.02 (\pm 0.90)$  in shallow and deep traps respectively with higher ratios in  
 319 the productive periods compared to the winter months. Mean POC:PN ratios were  $6.75 (\pm 0.46)$  and  
 320  $6.63 (\pm 0.71)$  during period 1 and period 2 in the shallow trap, and  $6.61 (\pm 0.65)$  and  $5.51 (\pm 0.87)$  in  
 321 the deep trap. Over the winter months POC:PN was  $5.68$  and  $5.92$  in shallow and deep traps  
 322 respectively.

323 BSi fluxes (Figure 3C) track those of POC well. Lowest fluxes ( $<20 \text{ mg SiO}_2 \text{ m}^{-2} \text{ d}^{-1}$ , except a small peak  
 324 of up to  $39.7 \text{ mg SiO}_2 \text{ m}^{-2} \text{ d}^{-1}$  in May 2018) occurred in the autumn/winter (March-October). During  
 325 summer 2018 (productive period 1), BSi fluxes were high, reaching  $129.1 \text{ mg SiO}_2 \text{ m}^{-2} \text{ d}^{-1}$  in early

326 February in the shallow trap and  $84.3 \text{ mg SiO}_2 \text{ m}^{-2} \text{ d}^{-1}$  in late February in the deep trap. By far the  
327 highest fluxes were observed in spring 2018 (productive period 2), peaking in early December at  
328  $562.4 \text{ mg SiO}_2 \text{ m}^{-2} \text{ d}^{-1}$ , and  $285.4 \text{ mg SiO}_2 \text{ m}^{-2} \text{ d}^{-1}$  in shallow and deep traps respectively. The mean  
329 BSi:POC ratio (mol:mol) throughout the study period was  $29.82 (\pm 17.80)$  and  $25.86 (\pm 11.72)$  in  
330 shallow and deep traps respectively. Higher BSi:POC ratios were observed in the shallow trap in  
331 period 1 ( $38.45 \pm 10.96$ ), and both shallow and deep traps in period 2 ( $36.94 \pm 16.32$  and  $35.70 \pm 12.10$   
332 respectively). BSi:POC ratios were lower in the deep trap during period 1 ( $23.64 \pm 6.82$ ). The match in  
333 timing of elevated fluxes of POC, PN and BSi fluxes in the shallow and deep traps in spring (period 2)  
334 highlights that sinking rates must be sufficient ( $>114 \text{ m d}^{-1}$ ) for particles to travel the 1600 m  
335 between the two traps in the 14 day period that those sediment trap cups were open. In period 1,  
336 there was a time lag of 14 to 35 days between the timing of the maximum POC, PN, and BSi fluxes in  
337 the deep and shallow sediment traps. This suggests sinking rates of 46-114  $\text{m d}^{-1}$ . However, we stress  
338 that this assumes vertical sinking, which as we discuss in Section 4 is not always the case.



340 **Figure 3: A) Particulate organic carbon (POC), B) particulate nitrogen (PN) and C) biogenic silica**  
 341 **(SiO<sub>2</sub>, BSi) fluxes (mg m<sup>-2</sup> d<sup>-1</sup>) at deep (red shading) and shallow (blue shading) sediment traps.**  
 342 **Shading indicates the maximum and minimum flux from two splits, with the solid line indicating**  
 343 **the mean value. Coloured points show isotope ratios for A) δ<sup>13</sup>C<sub>POC</sub>, B) δ<sup>15</sup>N<sub>PN</sub> and C) δ<sup>30</sup>Si<sub>BSi</sub> with red**  
 344 **open triangles and blue filled circles indicating deep and shallow sediment traps, respectively. The**  
 345 **maximum error on sediment trap δ<sup>13</sup>C<sub>POC</sub> (±1 ‰) and δ<sup>15</sup>N<sub>PN</sub> (±1.5 ‰) values are shown by scaled**  
 346 **error bars in the bottom right corner, and are associated with formaldehyde preservation (Mincks**  
 347 **et al., 2008) since this vastly exceeds analytical error. For δ<sup>30</sup>Si<sub>BSi</sub>, the scaled error bar represents 2**  
 348 **x SD (‰ 0.7) for the analytical sample replicates. For each sample, isotope ratios are given at the**  
 349 **midpoint of the period that the sample cup was open.**

### 350 3.3. δ<sup>13</sup>C<sub>POC</sub>, δ<sup>15</sup>N<sub>PN</sub> and δ<sup>30</sup>Si<sub>BSi</sub> Isotopes

351 δ<sup>13</sup>C<sub>POC</sub> values of deep and shallow sediment trap samples track each other well and show the same  
 352 order of enrichment and depletion (Figure 3A). Again, when presenting the results for an individual  
 353 sediment trap bottle, we give the mean of replicate splits from that sediment trap bottle unless  
 354 otherwise stated. Initially, from January to March 2018, we see isotopically light δ<sup>13</sup>C<sub>POC</sub> values  
 355 between -27.40 and -28.56 ‰, before increasing to -24.38 ‰ and -25.07 ‰ in June in shallow and  
 356 deep traps respectively. Over winter, δ<sup>13</sup>C<sub>POC</sub> became more depleted (shallow: -25.76 ‰ in October,  
 357 deep -27.07 ‰ in August) with a slight divergence (2.17 ‰) in the tracking of deep and shallow  
 358 δ<sup>13</sup>C<sub>POC</sub> in August 2018. Coinciding with increasing chlorophyll concentrations, δ<sup>13</sup>C<sub>POC</sub> became more  
 359 enriched during the period September to December 2018 (-25.72 to -21.13 ‰ and -26.04 to -21.98  
 360 ‰ for shallow and deep traps respectively).

361 Comparison of flux-weighted δ<sup>13</sup>C<sub>POC</sub> values confirms the carbon isotopic similarity of deep and  
 362 shallow traps, particularly during period 2 (Table 1). These results also highlight the shift in both  
 363 δ<sup>13</sup>C<sub>POC</sub> and δ<sup>30</sup>Si<sub>BSi</sub> between period 1 and period 2.

364 **Table 1: Sediment trap seasonal (Jan 2018-Dec 2018), period 1 (Jan 2018 – April 2018), and period**  
 365 **2 (Sept 2018-Dec 2018) flux-weighted mean δ<sup>13</sup>C<sub>POC</sub> (‰), δ<sup>15</sup>N<sub>PN</sub> (‰) and δ<sup>30</sup>Si<sub>BSi</sub> (‰) for shallow**  
 366 **(400 m) and deep (2000 m) traps. Given that the analytical conditions were the same for all**  
 367 **samples measured, we use the pooled variance over the applicable time period as a measure of**  
 368 **uncertainty on these mean isotopic ratios. Degrees of freedom (dof) are based on cups with**  
 369 **replicate isotopic measurements and are given in parentheses.**

Time period	δ <sup>13</sup> C <sub>POC</sub> (‰)		δ <sup>15</sup> N <sub>PN</sub> (‰)		δ <sup>30</sup> Si <sub>BSi</sub> (‰)	
	Shallow	Deep	Shallow	Deep	Shallow	Deep
Seasonal	-25.15 ±0.49 (dof=14)	-24.40 ±0.45 (dof=14)	2.07 ±0.34 (dof=14)	0.39 ±0.43 (dof=14)	0.50 ±0.09 (dof=8)	0.86 ±0.10 (dof=6)
Period 1	-28.30 ±0.31 (dof=5)	-27.52 ±0.33 (dof=5)	1.16 ±0.36 (dof=5)	0.73 ±0.58 (dof=5)	0.25 ±0.09 (dof=2)	0.47 ±0.13 (dof=2)
Period 2	-22.47 ±1.03 (dof=5)	-22.79 ±0.74 (dof=5)	2.97 ±0.66 (dof=5)	-0.09 ±0.65 (dof=5)	1.54 ±0.30 (dof=4)	1.08 ±0.14 (dof=4)

370

371  $\delta^{15}\text{N}_{\text{PN}}$  values are less consistent between deep and shallow sediment trap samples and there is  
372 more heterogeneity between sample splits. For the shallow trap we see values ranging between  
373 +0.13 and +2.96 ‰ (mean +1.42 ‰, SD 0.79 ‰) from January to June 2018, and, for the deep trap,  
374 values ranged between -1.95 and +3.04 ‰ (mean +0.60 ‰, SD 1.60 ‰) during this period. Values  
375 increase between June and August, reaching +5.42 and +2.10 ‰ in shallow and deep traps  
376 respectively. From August to December (shallow), and August to November (deep), we see a trend  
377 of decreasing  $\delta^{15}\text{N}_{\text{PN}}$  to +1.49 and -2.77 ‰ in shallow and deep traps respectively, with the decrease  
378 being of similar magnitude (3.93 and 4.87 respectively) for both traps. Shallow  $\delta^{15}\text{N}_{\text{PN}}$  are  
379 consistently higher than deep  $\delta^{15}\text{N}_{\text{PN}}$  by 4.52 ‰ on average during this period (August to November).  
380 In the deep trap we see a final increase in  $\delta^{15}\text{N}_{\text{PN}}$  coinciding with the increase in PN flux from  
381 November to December 2018, reaching a mean of +0.71 ‰. The same increase in  $\delta^{15}\text{N}_{\text{PN}}$  is not  
382 apparent in the shallow trap.

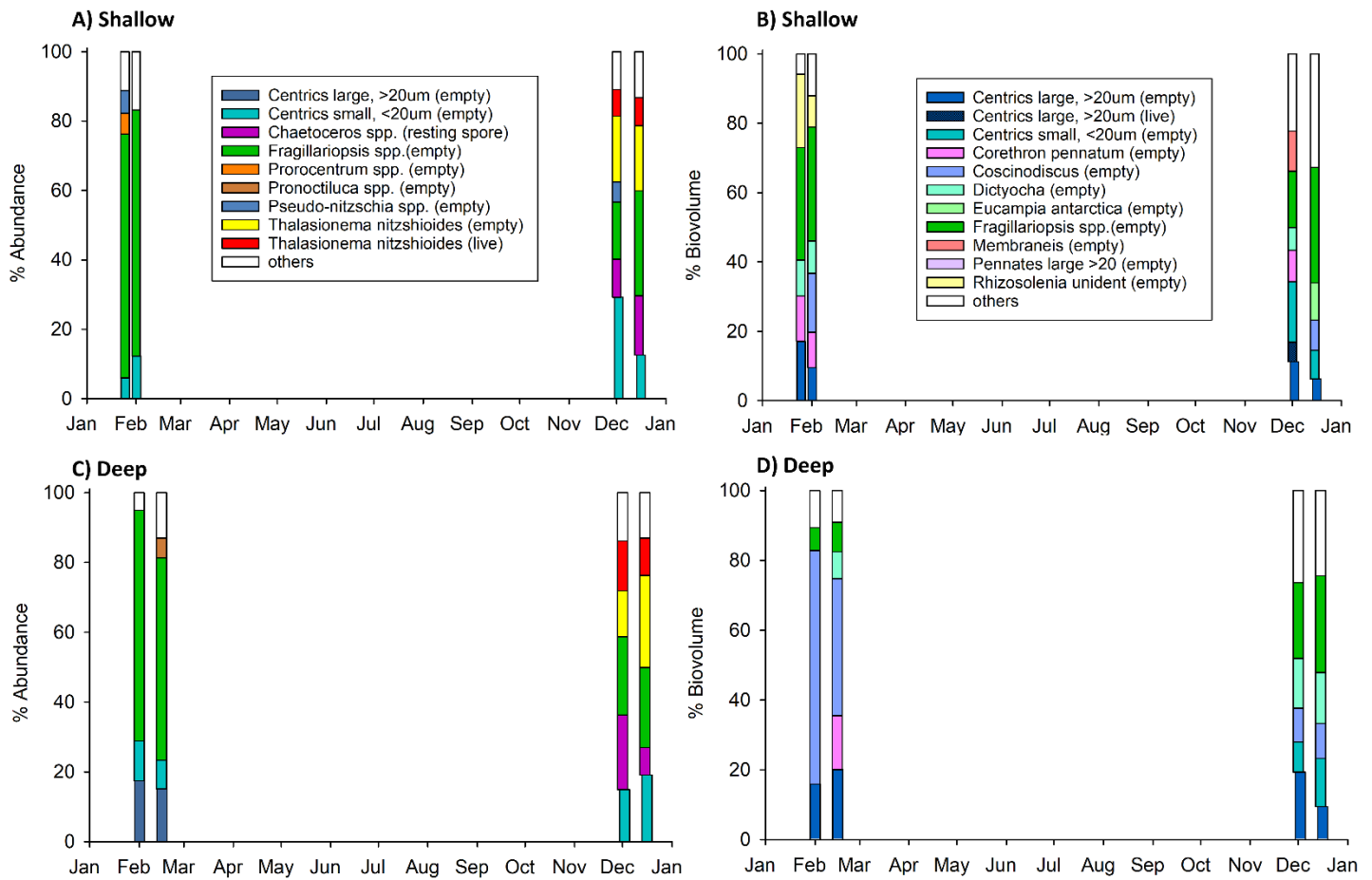
383 Si isotope compositions in deep and shallow samples were similar, exhibiting the same seasonal  
384 patterns. Both deep and shallow traps showed an increase in  $\delta^{30}\text{Si}_{\text{BSi}}$  from January to July 2018  
385 (+0.24 to +1.26 ‰) with the steepest increase occurring from March to May (Figure 3C). Sample  
386 splits generally showed good agreement with one exception during March 2018 when sample splits  
387 from the deep sediment trap were +0.52 and +1.41 ‰, highlighting the heterogeneous nature of the  
388 sediment trap material. Isotopic values were then quite steady over winter until the end of August  
389 when  $\delta^{30}\text{Si}_{\text{BSi}}$  began to decrease steeply, reaching +0.68 and +0.86 ‰ in shallow and deep traps  
390 respectively in November 2018. Following this,  $\delta^{30}\text{Si}_{\text{BSi}}$  increased rapidly to +1.72 (deep) and +1.89 ‰  
391 (shallow) coinciding with the large increase in BSi fluxes at this time.

#### 392 3.4. Phytoplankton community structure

393 Eight samples (four deep and four shallow, table 2) were analysed by light microscope for  
394 phytoplankton composition to cover the high productivity periods 1 and 2. Diatoms, silicoflagellates  
395 and dinoflagellates were observed, with a dominance of diatoms. Micro-zooplankton were also  
396 recorded, in particular radiolarian and tintinnids, though these were not dominant by biovolume or  
397 abundance. Only intact cells were identified and counted. In terms of abundance, during period 1,  
398 the diatoms *Fragilariopsis spp.* dominated both deep (58-66 %) and shallow (~70 %) trap samples  
399 (Figure 4A, C), whereas during period 2 the phytoplankton community structure was more mixed  
400 with contributions from the diatoms *Thalassionema nitzschioides*, *Chaetoceros*, small (<20  $\mu\text{m}$ )  
401 centrics, as well as *Fragilariopsis spp.* Large centric diatoms (>20  $\mu\text{m}$ ) represented 15-20 % of the  
402 community by abundance in the deep trap during productive period 1, but <2.5 % in productive  
403 period 2. Interestingly we do not see these large centrics in the shallow trap during productive  
404 period 1, implying that sinking velocities were < 76  $\text{m d}^{-1}$  for these large phytoplankton cells based on  
405 the duration that the first sediment trap bottle was open and the depth between the two traps.

406 In terms of biovolume, *Fragilariopsis spp.* were still a dominant component of the shallow trap  
407 sample in period 1 (~33 %) but were <9 % of the community in the deep trap during period 1, with  
408 the large cells of the diatom *Coscinodiscus* dominating 39-67 % (Figure 4B, D). Diatoms, *Corethron*  
409 *pennatum* (shallow: 10-13 %; deep: 15 %), *Rhizosolenia* (shallow: 9-21 %), and large centric diatoms  
410 (>20  $\mu\text{m}$ ) (shallow: 10-17 %; deep: 16-20 %), as well as the silicoflagellate *Dictyochoa* (shallow: 9-10 %;  
411 deep: 8 %), were also relatively high in terms of biovolume during period 1. During period 2, the  
412 community in terms of biovolume was quite mixed in the shallow trap (Figure 4B), with similar

413 contributions from *Fragilariopsis* spp. (22-28 %), *Dictyocha* (14-15 %), *Coscinodiscus* (10 %), and,  
 414 small (<20 μm, 9-14 %) and large (>20 μm, 9-19 %) centric diatoms in the deep trap.



416 **Figure 4: Phytoplankton assemblage of A,B) shallow and C, D) deep sediment trap samples,**  
 417 **according to abundance (A, C) and biovolume (B, D). Plots A and C show phytoplankton**  
 418 **contributing >5 % by abundance, and plots B and D show >5 % by biovolume. Four samples were**  
 419 **identified taxonomically for each trap. Note that only intact cells were counted.**

420

#### 421 4. Discussion

422 In this study we measure the seasonal cycle of POC, PN and BSi fluxes as well as the  $\delta^{13}\text{C}_{\text{POC}}$ ,  $\delta^{15}\text{N}_{\text{PN}}$   
423 and  $\delta^{30}\text{Si}_{\text{BSi}}$  values of sinking particles collected in shallow (400 m) and deep (2000 m) sediment traps  
424 in the Scotia Sea, Southern Ocean. Both the magnitude and isotopic compositions were generally  
425 similar in the shallow and deep sediment traps, suggesting that most remineralisation occurred in  
426 the upper 400 m. This highlights that material reaching 400 m likely facilitates the transfer of carbon  
427 much deeper in the ocean, sequestering carbon for longer time periods (Kwon et al., 2009).

##### 428 4.1. Seasonal flux cycles

429 The seasonal cycles of POC agree well with previously published work at the same location (Manno  
430 et al., 2015), with peaks in austral spring and late summer, though the peak POC fluxes recorded  
431 here (45.7 mg C m<sup>-2</sup> d<sup>-1</sup> and 43.4 mg C m<sup>-2</sup> d<sup>-1</sup>, in shallow and deep traps respectively) are higher than  
432 those observed in previous years (22.9 mg C m<sup>-2</sup> d<sup>-1</sup>; Manno et al., 2015). A smaller additional peak in  
433 POC flux (<10 mg C m<sup>-2</sup> d<sup>-1</sup>) occurred in April/May, in agreement with some previous years (Manno et  
434 al., 2015). PN fluxes followed the same seasonal trend as POC for both deep and shallow traps  
435 suggesting a similar source. The similar magnitude of POC:PN ratios in period 1 in the two traps  
436 support consistency in the degree of degradation at these depths. The lower POC:PN ratios  
437 measured in the deep trap between August and October, compared to the shallow trap are  
438 consistent with a divergence in  $\delta^{15}\text{N}_{\text{PN}}$  ratios, and could relate to a change in source material and/or  
439 degradation state between the two traps at this time.

440 Our measured fluxes of BSi are higher than previously observed at this site at 2000 m in 2012  
441 (Rembauville et al., 2016). Maximum fluxes of 46.0 mg SiO<sub>2</sub> m<sup>-2</sup> d<sup>-1</sup> were recorded by Rembauville et  
442 al. (2016) in January 2012, which though of similar magnitude to our summer peak of 84.3 mg SiO<sub>2</sub>  
443 m<sup>-2</sup> d<sup>-1</sup>, is an order of magnitude lower than the spring peak of 285.4 mg SiO<sub>2</sub> m<sup>-2</sup> d<sup>-1</sup> in December  
444 2018. However, the Rembauville et al. (2016) record ends in November and therefore would not  
445 have captured the main peak in particle flux following the phytoplankton spring bloom in December  
446 (apparent in satellite surface chlorophyll, Figure 2 in Rembauville et al., 2016). Additionally, we do  
447 not capture the first 3 weeks of January in our data. Closset et al. (2015) measured very high fluxes  
448 (>700 mg SiO<sub>2</sub> m<sup>-2</sup> d<sup>-1</sup>) of BSi south of the Polar Front in the Australian sector of the Southern Ocean  
449 at 2000 m, and similarly high fluxes have been observed in other sectors (Fischer et al., 2002; Honjo  
450 et al., 2000).

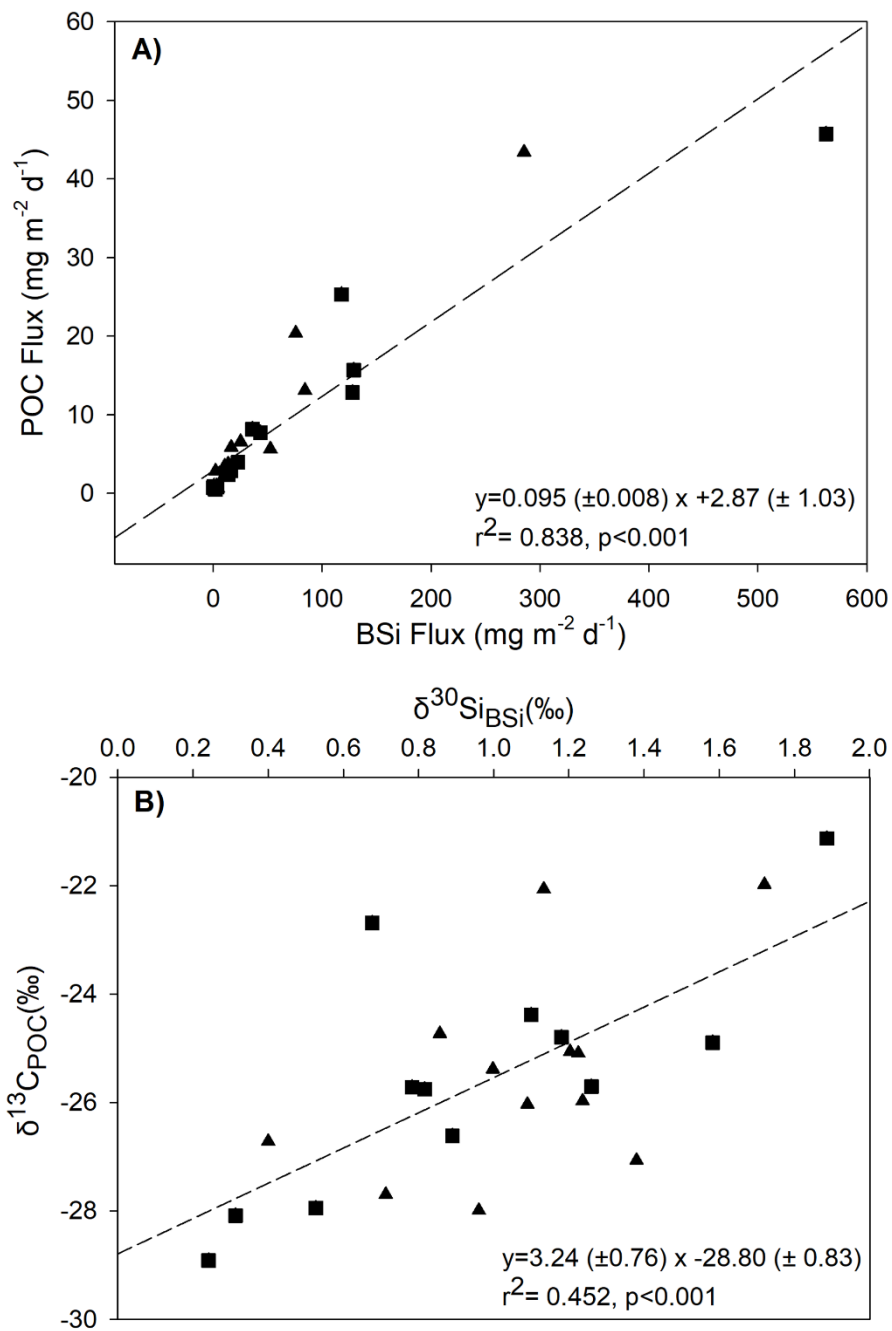
451 We define two main productive periods, productive period 1 from January to April 2018, and  
452 productive period 2 from September to December 2018 when chlorophyll concentrations were >0.4  
453 mg m<sup>-3</sup>. Satellite data suggest the magnitude of chlorophyll concentration was similar during both  
454 productive periods, but increasing in magnitude throughout period 2, and decreasing in period 1,  
455 consistent with timing of sampling. The particle fluxes associated with productive period 2 were  
456 much higher than those during productive period 1, a difference which is particularly pronounced for  
457 BSi fluxes. The bloom during period 2 was more geographically widespread (Figure S2) and thus it is  
458 possible that if more of the material reaching the trap was sourced from productive waters, this  
459 could have supported the higher fluxes observed at this time. The observed higher BSi fluxes in  
460 productive period 2 could also relate to the presence of more heavily silicified diatom species at this  
461 time, including the occurrence of resting spores (*Chaetoceros spp.*; Figure 4, and Rembauville et al.  
462 (2016)), increased aggregation (and thus sinking) potential, higher sinking rates, and/or reduced

463 grazing pressure. The fact that we observed resting spores at the end of productive period 2,  
464 suggests that nutrients may have started to become limiting for at least some of the phytoplankton  
465 community (e.g. silicic acid and/or iron, Rembauville et al., 2016). POC and BSi fluxes track each  
466 other closely and ratios suggest high export of biogenic silica (Figure 5). This, combined with our  
467 visual observations of a dominance of algal material in the trap during the spring peak that was  
468 dominated by diatoms (Figure 4), suggest an important role for diatoms in transferring organic  
469 carbon to the deep ocean at this time. This could be achieved if cells are large through large mineral  
470 (silica) ballasted cells sinking at high velocities (Baumann et al., 2022), or through the bioprotection  
471 of internal organic matter from grazing and oxidation by the diatom silica frustules (Passow and De  
472 La Rocha, 2006; Armstrong et al., 2001; Smetacek et al., 2004).

#### 473 *4.2. Seasonal variations in isotope ratios*

474 In terms of the seasonality, we see broadly similar trends for both  $\delta^{13}\text{C}_{\text{POC}}$  and  $\delta^{30}\text{Si}_{\text{BSi}}$  (linear  
475 regression,  $R^2 = 0.452$ ,  $p < 0.001$ , Figure 5), again highlighting the close coupling of carbon and silicon  
476 cycling processes. We do not find significant relationships between  $\delta^{15}\text{N}_{\text{PN}}$  and  $\delta^{13}\text{C}_{\text{POC}}$  or  $\delta^{30}\text{Si}_{\text{BSi}}$ . We  
477 break the season into 3 main periods for discussion, productive period 1 (first export event), the  
478 winter flux hiatus, and productive period 2 (second export event).





479

480 **Figure 5: Relationship between BSi and POC for data from both deep (triangles) and shallow**  
 481 **(squares) sediment traps. A) Regression between BSi and POC fluxes, and B) between  $\delta^{13}\text{C}_{\text{POC}}$  and**  
 482  **$\delta^{30}\text{Si}_{\text{BSi}}$ . Regression lines are shown by dotted lines with coefficients and associated standard errors**  
 483 **also shown.**

484

485 4.2.1. Productive period 1

486

487 During productive period 1,  $\delta^{13}\text{C}_{\text{POC}}$  is low, averaging -28.30 and -27.52 ‰ in shallow and deep traps  
488 respectively, close to that expected for Southern Ocean phytoplankton employing typical C3  
489 metabolism (i.e. diffusive  $\text{CO}_2$  transfer into the internal cell pool and Rubisco carboxylation) (Raven,  
490 1997). This is consistent with the dominance of diatoms (*Fragilariopsis spp.*) in the trap material, as  
491 Bacillariophyceae are known to employ C3 metabolism (Table IV in Raven 1997). Preferential uptake  
492 of  $^{28}\text{Si}$  by diatoms (De La Rocha et al., 1997) during the late spring bloom of productive period 1 also  
493 explains the low  $\delta^{30}\text{Si}_{\text{BSi}}$  values. BSi:POC ratios were elevated at the start of productive period 1,  
494 suggesting that phytoplankton were heavily silicified. After initial low values, we see a progressive  
495 increase in both  $\delta^{13}\text{C}_{\text{POC}}$  and  $\delta^{30}\text{Si}_{\text{BSi}}$ , reflecting the progressive utilisation of both  $^{12}\text{C}$  and  $^{28}\text{Si}$  as  
496 nutrient pools are consumed during the bloom. As such, the diatom cells reaching the sediment trap  
497 in late spring/summer were utilising increasingly isotopically-enriched C and Si for growth leading to  
498 progressive isotopic enrichment of the cells sinking into the sediment trap. This observation fits with  
499 elevated but decreasing surface chlorophyll concentrations from February to April 2018. Increasing  
500  $\delta^{13}\text{C}_{\text{POC}}$  and  $\delta^{30}\text{Si}_{\text{BSi}}$  into the late summer may also partially reflect preferential remineralisation of the  
501 more labile  $^{12}\text{C}$  and  $^{28}\text{Si}$  in particles as they sink through the upper 400 m of the water column. The  
502 lack of variation in  $\delta^{13}\text{C}_{\text{POC}}$  and  $\delta^{30}\text{Si}_{\text{BSi}}$  between 400 and 2000 m in our study suggests this may be  
503 limited over these depth ranges, or that there is no fractionation effect. Whilst laboratory-based  
504 silica dissolution experiments are equivocal (Demarest et al., 2009; Wetzel et al., 2014), our findings  
505 agree with field studies that also indicate a lack of Si isotopic fractionation during diatom silica  
506 dissolution (Closset et al., 2015; Egan et al., 2012).

507 During productive period 1 there was no clear trend in  $\delta^{15}\text{N}_{\text{PN}}$ , with values between -1.95 and +2.96  
508 ‰. We speculate that this mixed signal with no significant difference between deep and shallow  
509 traps resulted from a combination of surface phytoplankton using both ammonium and nitrate as  
510 the inorganic nitrogen source, and variability in the sediment trap material composition.  
511 Enrichments of 2-4 ‰ occur between successive trophic levels, and egestion and excretion can have  
512 varying isotopic effects (see Section 4.3), thus the presence of faecal pellets, animal moults and  
513 carcasses could alter the isotopic composition of the sediment trap material. Additionally, any supply  
514 of ammonium through remineralisation would be utilised quickly because ammonium is kinetically  
515 favourable to nitrate (Glibert et al., 2016), resulting in particles with a decreased  $\delta^{15}\text{N}_{\text{PN}}$  compared to  
516 those produced by nitrate assimilation.

517

#### 518 4.2.2. Winter hiatus

519 Between May and August, both  $\delta^{13}\text{C}_{\text{POC}}$  and  $\delta^{30}\text{Si}_{\text{BSi}}$  showed little change, with a slight progressive  
520 decrease for  $\delta^{13}\text{C}_{\text{POC}}$  and slight increase in  $\delta^{30}\text{Si}_{\text{BSi}}$ . It is possible that the slight progressive trend  
521 towards a lighter carbon isotopic composition of sinking particles from -24.94 to -25.98 ‰ is driven  
522 by a mixture of older, isotopically heavier particles that have undergone partial remineralisation and  
523 the input of material of different isotopic composition from the small secondary peak in POC we  
524 observed in April/May. An input of smaller, more slowly sinking cells reaching the trap in increasing  
525 numbers following the initial late spring peak in production could drive the lower  $\delta^{13}\text{C}_{\text{POC}}$  at this time.  
526 Additionally, the pulse of material could be driven by a successive peak in production of a different  
527 phytoplankton community with a different isotopic signature. Korb et al. (2012) found an increasing  
528 presence of dinoflagellates from spring to summer, as well as seasonal changes in the size structure  
529 of the phytoplankton community to the northwest of South Georgia, supporting either hypothesis.

530 We do not have the species composition data from this time period to evidence this directly, but we  
531 suggest that the reduction in  $\delta^{13}\text{C}_{\text{POC}}$  does not relate to a mixing event and a resupply of  $^{12}\text{C}$ , due to  
532 the fact that  $\delta^{30}\text{Si}_{\text{BSi}}$  continued to increase slowly. Given the generally lighter silicon isotopic  
533 composition of seawater below the photic zone, we would expect a mixing event to also result in a  
534 decline in seawater  $\delta^{30}\text{Si}$  and consequently  $\delta^{30}\text{Si}_{\text{BSi}}$ . This would mean that our hypothesised shift in  
535 phytoplankton species composition in the traps (May-August) did not impact Si fractionation to the  
536 same extent as carbon isotopes. Whereas size, growth rates, cell geometry and different carbon  
537 acquisition mechanisms have all been highlighted as impacting the  $\delta^{13}\text{C}_{\text{POC}}$  of marine plankton (Popp  
538 et al., 1999, 1998; Bidigare et al., 1999; Trull and Armand, 2001; Tuerena et al., 2019), species  
539 dependent Si fractionation by polar and subpolar diatoms has only been observed in the laboratory,  
540 not in the field (Annett et al., 2017; Cassarino et al., 2017; Sutton et al., 2013).  $\delta^{15}\text{N}_{\text{PN}}$  in the shallow  
541 trap showed a slight progressive decrease over the winter period, before increasing in August to  
542 5.42 ‰. The progressive decrease is consistent with the propagation of the surface signal of  
543 phytoplankton growth and fractionation, with increasing influence of ammonium uptake as the  
544 season progresses that leads to low  $\delta^{15}\text{N}_{\text{PN}}$ . The large range in  $\delta^{15}\text{N}_{\text{PN}}$  in the deep trap in July makes it  
545 difficult to determine with certainty a trend in  $\delta^{15}\text{N}_{\text{PN}}$  in the deep trap between July and October.

546

#### 547 *4.2.3. Productive period 2*

548 At the start of productive period 2 (September) we saw a significant decrease in  $\delta^{30}\text{Si}_{\text{BSi}}$  (~0.5 ‰) in  
549 both traps suggesting resupply of  $^{28}\text{Si}$  enriched silicic acid to the euphotic zone via mixing.  
550 Interestingly, we did not see the same consistent shift in carbon isotopes; we measured a ~1 ‰  
551 decrease in the shallow trap  $\delta^{13}\text{C}_{\text{POC}}$  and a ~1 ‰ increase in the deep trap  $\delta^{13}\text{C}_{\text{POC}}$ . We speculate that  
552 this mixing could bring waters of increased silicic acid concentrations to the surface, promoting full  
553 expression of the isotope fractionation effect from phytoplankton uptake and thus lower  $\delta^{30}\text{Si}_{\text{BSi}}$  in  
554 sinking particles. To match our observations, these mixed waters would need to be similar in  
555 dissolved inorganic carbon concentrations and  $\delta^{13}\text{C}$ , which could relate to the depth of mixing and  
556 differences in the depth at which POC and BSi are remineralised (Friedrich and Rutgers van der Loeff,  
557 2002; Weir et al., 2020). We note that current velocities recorded at this time were elevated (Figure  
558 S1), particularly in the deep trap, suggesting a shift in the surrounding velocity fields, which may  
559 have resulted in biased sample collection at this time through either over or under collection  
560 (Buesseler et al., 2007). Whereas  $\delta^{13}\text{C}_{\text{POC}}$  progressively increased during productive period 2, from -  
561 25.88 ‰ in September to -21.56 ‰ at the end of December (mean of deep and shallow traps),  
562  $\delta^{30}\text{Si}_{\text{BSi}}$  continued to decrease until November before showing a sudden increase from +0.74 ‰ to  
563 +1.80 ‰ at the end of the sampling period. This may suggest that DSi, or co-limiting nutrients, was  
564 replete, and uptake could occur unhindered until November 2018 when very high rates of  
565 production and the associated high fluxes of BSi increased the demand for DSi and led to enrichment  
566 of  $\delta^{30}\text{Si}$  in overlying waters and subsequently sinking siliceous phytoplankton. For carbon, uptake  
567 was sufficient from September to progressively deplete source waters in  $^{12}\text{C}$ , driving an increase in  
568  $\delta^{13}\text{C}$  in surface waters and newly formed phytoplankton cells. BSi:POC ratios increased from  
569 September to December suggesting that material reaching the traps was increasingly silicified.

570 Interestingly, unlike C and Si isotopes, we saw a divergence in the nitrogen isotopic composition of  
571 deep and shallow traps between August and December. The sharp increase in mean  $\delta^{15}\text{N}_{\text{PN}}$  from  
572 +1.32 ‰ in July to +5.42 ‰ in August 2018 in the shallow trap that initiated the divergence strongly

573 suggests an advective change in source material. As noted above, this was a period of increased  
574 horizontal velocities and may have facilitated material reaching the two traps from different sources  
575 of differing initial composition and degradation states. The substantially lower  $\delta^{15}\text{N}_{\text{PN}}$  in the deep  
576 trap from August to November, compared to that of the shallow trap is surprising. It would be  
577 expected, that, as particles sink and are progressively decomposed this would remove dissolved  
578 nitrogen depleted in  $^{15}\text{N}$ , thus increasing  $\delta^{15}\text{N}_{\text{PN}}$  in the particles. Indeed many studies have observed  
579 this trend of increasing  $\delta^{15}\text{N}$  with depth in suspended particles (Altabet et al., 1991 and references  
580 therein). However, like Altabet et al. (1991), we observe lower  $\delta^{15}\text{N}_{\text{PN}}$  in sinking particles in the deep  
581 sediment trap. This has also been observed previously in Antarctic waters (Wada et al., 1987).  
582 Though the reason for this is not well understood (Sigman and Fripiat, 2019), it appears to be a  
583 consistent phenomenon. Particles in our deep trap must therefore be gaining light nitrogen or losing  
584 heavy nitrogen and could reflect a different source composition. In agreement with Altabet et al.  
585 (1991), we suggest that lateral transport of low  $\delta^{15}\text{N}_{\text{PN}}$  from a region of increased ammonium-based  
586 production could explain this, highlighting a difference in the source of sinking particles to the two  
587 traps. Altabet et al. (1991) also suggests that, since protein nitrogen is 3 ‰ higher than bulk  
588 nitrogen, the selective decomposition of protein could explain the decrease in  $\delta^{15}\text{N}$  with depth,  
589 though why this would not be the case also for suspended PN is unclear. We observe the greatest  
590 divergence in shallow and deep N isotope compositions during periods of low PN flux (Figure 3),  
591 consistent with the observations of Altabet et al. (1991), enabling a low flux of laterally supplied  
592 material to have an amplified impact on the isotope signal. In support of this, in December when  
593 particle fluxes increase sharply with the spring bloom,  $\delta^{15}\text{N}_{\text{PN}}$  in the deep trap increases more in line  
594 with that of the shallow trap, highlighting a switch from source material being dominated by lateral  
595 supply when vertical supply is negligible, to the dominance of vertical supply from surface  
596 production following the phytoplankton bloom.

597

#### 598 4.3. Drivers of a shifting isotopic ratios

599 The mean flux-weighted isotopic composition measured during productive periods 1 (January to  
600 April 2018) and 2 (September to December 2018) suggests that the processes driving the flux of  
601 material at these times differ (Figure 3, Table 1). The divergence in the  $\delta^{15}\text{N}_{\text{PN}}$  of deep and shallow  
602 trap material during period 2 limits our ability to compare the temporal shifts in mean isotopic ratios  
603 for nitrogen isotopes, so we focus here on  $\delta^{13}\text{C}_{\text{POC}}$  and  $\delta^{30}\text{Si}_{\text{BSi}}$ . Since our record does not extend  
604 beyond December 2018, and we do not capture the first 3 weeks of January 2018 when fluxes are  
605 likely high, we do not record the initial value at this time, however, we would expect  $\delta^{13}\text{C}_{\text{POC}}$  to be  
606 even more negative at this time. We cannot determine if  $\delta^{13}\text{C}_{\text{POC}}$  and  $\delta^{30}\text{Si}_{\text{BSi}}$  would return to values  
607 akin to that in period 1 in the following late spring-summer season (January 2019). We saw a shift in  
608  $\delta^{13}\text{C}_{\text{POC}}$  from a mean of -28.31 ‰ in January 2018 at the time of our first measurements to -25.88 ‰  
609 in September at the start of period 2. This coincided with a change in community structure, with  
610 abundance dominated by *Fragilariopsis spp.* in period 1 to a more mixed community in period 2. Of  
611 the abundant phytoplankton species (>5%, Figure 4A, C), we find statistically significant linear  
612 relationships between  $\delta^{13}\text{C}_{\text{POC}}$  and percent abundance for *Fragilariopsis spp.* (empty:  $R^2 = 0.926$ ,  
613  $p < 0.001$ ), *Thalassionema nitzschioides* (live:  $R^2 = 0.774$ ,  $p = 0.004$ ; empty:  $R^2 = 0.844$ ,  $p = 0.001$ ), and  
614 *Chaetoceros spp. (resting spore)* ( $R^2 = 0.732$ ,  $p = 0.007$ ). We stress this is based on only 8 samples.  
615 Nevertheless, these robust samples show that there was a shift in phytoplankton community

616 structure. Though *Fragilariopsis spp.* were mainly empty cells, colonisation by bacteria (Grossart et  
 617 al., 2003; Kjørboe et al., 2003) may facilitate carbon transfer within and on these cells, and certainly  
 618 the live cells of *T. nitzschioides* and resting spores of *Chaetoceros spp.* would act as agents of carbon  
 619 transfer (Agusti et al., 2015; Salter et al., 2012; Rembauville et al., 2016).

620 We examine whether this shift in phytoplankton community composition is associated with a change  
 621 in SA:V (Table 2) since greater fractionation of carbon in smaller phytoplankton cells with higher  
 622 SA:V is well observed in the literature (e.g. Popp et al., 1998; Tuerena et al., 2019). There was a  
 623 statistically significant (paired t-test,  $p=0.008$ ) difference in the community SA:V between productive  
 624 periods, increasing from  $0.35 \mu\text{m}^2 \mu\text{m}^{-3}$  in period 1 to  $0.51 \mu\text{m}^2 \mu\text{m}^{-3}$  in period 2. However, this would  
 625 result in increased isotopic fractionation during period 2, in opposition to what we observed. We  
 626 note here, that as only intact cells were counted, the measured SA:V ratios may not fully account for  
 627 the isotopic composition of the trap material due to the presence of fragmented material. It is  
 628 possible that there was a change in the mechanism of carbon uptake with the more mixed  
 629 phytoplankton community in period 2 using  $\text{HCO}_3^-$  instead of  $\text{CO}_2$  or employing carbon concentrating  
 630 mechanisms (CCMs), both of which would result in higher  $\delta^{13}\text{C}_{\text{POC}}$  than the diffusive uptake of  $\text{CO}_2$  via  
 631 Rubisco (Raven, 1997; Cassar et al., 2004). Studies show that there is much diversity amongst  
 632 diatoms in the use of CCMs and many are able to take up both  $\text{CO}_2$  and  $\text{HCO}_3^-$  (Trimborn et al., 2009;  
 633 Roberts et al., 2007; Shen et al., 2017; Young et al., 2016). We suggest that species driven  
 634 differences in carbon uptake mechanisms account in part for the differing  $\delta^{13}\text{C}_{\text{POC}}$  that we observed  
 635 during the two main productive periods.

636 **Table 2: Phytoplankton cell community surface area to volume (SA:V) ratios measured in deep and**  
 637 **shallow sediment traps for samples enumerated in both productive periods 1 and 2.**

Bottle open date	Depth	Period	Mean community SA:V
25/01/2018	Shallow	1	0.39
01/02/2018	Shallow	1	0.35
01/02/2018	Deep	1	0.33
15/02/2018	Deep	1	0.32
01/12/2018	Deep	2	0.53
01/12/2018	Shallow	2	0.48
15/12/2018	Deep	2	0.53
15/12/2018	Shallow	2	0.52

638 We also observed a shift in the mean flux-weighted  $\delta^{30}\text{Si}_{\text{BSi}}$  ratios (Table 1) between period 1 and  
 639 period 2. With the exception of one culture study (Sutton et al., 2013), systematic species driven  
 640 shifts in  $\delta^{30}\text{Si}_{\text{BSi}}$  fractionation have not been observed (e.g., De La Rocha et al., 1997), suggesting that  
 641 there may be an additional driver of the changing isotopic ratios. Since, prior to our first  
 642 measurements there had been a long-lasting phytoplankton bloom (Figure S2), we would expect  
 643 production to have utilised much of the light  $^{28}\text{Si}$ , resulting in particles with enriched  $\delta^{30}\text{Si}_{\text{BSi}}$  reaching  
 644 the trap in January 2018. However, we observe isotopically light mean values of  $+0.48 \text{‰}$  at the start  
 645 of sampling at the end of January, suggesting that there must have been a resupply of  $^{28}\text{Si}$ . Physical  
 646 mixing, bringing deep and benthic waters rich in nutrients, including iron, to the surface waters  
 647 around South Georgia, are known to support the large blooms occurring downstream of South  
 648 Georgia (Matano et al., 2020; Nielsdóttir et al., 2012) and could supply both  $^{12}\text{C}$ -enriched dissolved  
 649 inorganic carbon and  $^{28}\text{Si}$ -enriched silicic acid. Additional nutrients could also be supplied to our

650 study region by glacial discharge associated with isotopically light silicon isotopic signatures (Matano  
651 et al., 2020; Hatton et al., 2019), or benthic fluxes from shelf sediments, likely also releasing  
652 isotopically light DSi (Ng et al., 2020; Cassarino et al., 2020; Closset et al., 2022). Therefore, we  
653 suggest that low values (increased fractionation) of  $\delta^{13}\text{C}_{\text{POC}}$  and  $\delta^{30}\text{Si}_{\text{BSi}}$  during period 1 relate to  
654 increased nutrient availability enabling full expression of the isotopic fractionation and thus  
655 isotopically light particulate material to reach the sediment trap.

656 The ocean circulation in our study region is complex and variable on fine spatial and temporal scales,  
657 affecting horizontal and vertical velocities (e.g. Boehme et al., 2008). It is clear from the currents  
658 measured at the depths of our two traps (Figure S1), that both the direction and magnitude of the  
659 flow can vary within and between seasons and is not necessarily consistent between the two depths.  
660 There are thus potentially different source regions for material in the two traps at certain times of  
661 the year. We lack the full depth resolution of vertical and horizontal velocity fields and information  
662 on sinking rates to confirm this, but previous studies have highlighted variability in the locations of  
663 the Southern Antarctic Circumpolar Current Front and the Polar Front, as well as eddies generated  
664 from these fronts, in our study region (Moore et al., 1999; Boehme et al., 2008; Whitehouse et al.,  
665 1996). We suggest that variability in ocean current velocities could explain different isotopic ratios in  
666 period 1 and 2, through the supply of material to the traps from different source region with  
667 differing nutrient and remineralisation regimes. Different source waters would impact nutrient  
668 availability including iron supply, uptake and recycling (Hawco et al., 2021; Ellwood et al., 2020),  
669 which in turn influences species composition, nutrient utilisation and uptake rates (e.g. Meyerink et  
670 al., 2019). This highlights the importance of making synchronous, and full depth resolution  
671 measurements of, physical processes such as current strength and direction, to be able to distinguish  
672 between spatial and temporal drivers of shifts in species composition, particle flux and isotopic  
673 composition.

674 Since trophic transfer is known to impact both carbon and nitrogen isotope compositions of organic  
675 matter, the presence of moults and faecal pellets in trap samples are also important to consider. An  
676 incubation study focussed on *Euphausia superba* found that the  $\delta^{15}\text{N}$  of the *E. superba* faecal pellets  
677 was always lower than that of the copepods they ingested, though still higher than that of POM  
678 (Schmidt et al., 2003). Additionally, Tamelander et al. (2006) measured faecal pellets produced by  
679 copepods with depleted  $^{15}\text{N}$  compared to the algal food source. Though a few studies on temperate  
680 and subtropical copepods showed that the faecal material had similar or slightly higher  $\delta^{15}\text{N}$  than  
681 the food source (Altabet and Small, 1990; Checkley and Entzeroth, 1985), there is not a consistent  
682 fractionation effect of egestion, for either  $\delta^{15}\text{N}$  or  $\delta^{13}\text{C}$ , which may relate to compositional  
683 differences (protein, carbohydrate, lipid) and their isotopic values (Tamelander et al., 2006). We are  
684 therefore not able to determine the impact of faecal pellets or moults on the isotopic composition of  
685 our samples. As phytoplankton material dominated at the times of peak flux, we suggest that the  
686 importance of faecal pellets and moults may be greater during periods of lower flux, however we  
687 cannot rule out their contribution during the bloom periods. We suggest that it would be highly  
688 informative to conduct particle specific isotope analysis of common particle types in sediment traps  
689 such as faecal pellets, phytoplankton detritus and zooplankton moults, to improve our ability to  
690 determine the impact of particle flux composition on bulk isotope compositions.

691

692 **Conclusion**

693 The seasonal cycles in primary productivity and nutrient uptake in surface waters at our study site in  
694 the Scotia Sea are reflected in the fluxes and isotopic ratios of sinking particulate material. We find  
695 that most remineralisation occurs in the upper 400 m of the water column and below this the  
696 magnitude of the flux of sinking material is relatively consistent, supported by consistency in  
697 POC:PON ratios. We find that particulate fluxes of C, and BSi are tightly coupled which highlights the  
698 importance of siliceous material in the transfer of POC to depth. We suggest that a change in  
699 phytoplankton community structure can at least part explain the shifts in carbon isotopic  
700 composition between the two productive periods measured here. Though complex, seasonal  
701 patterns in isotopic composition of particulate material reaching the sediment traps do reflect the  
702 degree and type of nutrient utilisation in the source waters. Our data also suggests an importance of  
703 laterally supplied material to the sediment traps and supports seasonal differences in source  
704 regions. Our results highlight how, through more detailed mechanistic understanding of the drivers  
705 of POC flux, and biogeochemical cycling, we can improve estimates of the current and future  
706 strength of the biological carbon pump and the ocean's role as a CO<sub>2</sub> sink.

707

#### 708 **Data availability**

709 Phytoplankton abundances and biovolume, as well as mean flux and isotopic ratios are available  
710 with the following DOI's:

711 DOI in progress with the British Antarctic Survey Polar Data Centre

#### 712 **Author contributions**

713 AB and CM conceived the study and participated in fieldwork to collect samples. AB conducted  
714 laboratory analysis with support from TW, LF, and UD for isotope analysis. MW conducted  
715 phytoplankton analysis and provided intellectual input on phytoplankton community composition.  
716 SH and KH provided support for isotopic analysis and contributed to the interpretation of the data  
717 and implications. CC supported uncertainty analysis. All authors contributed text to the manuscript.

#### 718 **Competing Interests**

719 The authors declare that they have no conflict of interest.

720

#### 721 **Acknowledgements**

722 We are very grateful to the scientists and crew aboard research cruises JR17002 and DY098 for their  
723 efforts to deploy and recover the P3 mooring. We thank staff at the Bristol Isotope Group for  
724 running and maintenance of the mass spectrometer facilities at the University of Bristol, as well as  
725 Colin Chilcott for technical support for C and N analysis at the University of Edinburgh. AB and CM  
726 were supported by NC-ALI funding and ecosystems programme. CM was also funded by UKRI FLF  
727 project MR/T020962/1. SH was supported by the United Kingdom Natural Environment Research  
728 Council through grant NE/K010034/1. UD was supported by the UK NERC through grant  
729 NE/P006108/1. LF was supported by a NERC GW4+ DTP studentship and TW by a CSC-UoB Joint  
730 Scholarship. We thank Sally Thorpe and Emma Young for insights on the physical oceanographic

731 conditions of the region. Finally, a special thanks to Flo Atherden for her dedicated work picking out  
732 swimmers from the shallow sediment trap.

733

#### 734 **References**

735 Agustí, S., González-Gordillo, J. I., Vaqué, D., Estrada, M., Cerezo, M. I., Salazar, G., Gasol, J. M., and  
736 Duarte, C. M.: Ubiquitous healthy diatoms in the deep sea confirm deep carbon injection by the  
737 biological pump, *Nat. Commun.*, 6, 1–8, <https://doi.org/10.1038/ncomms8608>, 2015.

738 Altabet, M. A. and Small, L. F.: Nitrogen isotopic ratios in fecal pellets produced by marine  
739 Zooplankton, *Geochim. Cosmochim. Acta*, 54, 155–163, [https://doi.org/10.1016/0016-7037\(90\)90203-W](https://doi.org/10.1016/0016-7037(90)90203-W), 1990.

741 Altabet, M. A., Deuser, W. G., Honjo, S., and Stienen, C.: Seasonal and depth-related changes in the  
742 source of sinking particles in the North Atlantic, *Nature*, 354, 136–139,  
743 <https://doi.org/10.1038/354136a0>, 1991.

744 Annett, A. L., Henley, S. F., Venables, H. J., Meredith, M. P., Clarke, A., and Ganeshram, R. S.: Silica  
745 cycling and isotopic composition in northern Marguerite Bay on the rapidly-warming western  
746 Antarctic Peninsula, *Deep. Res. Part II Top. Stud. Oceanogr.*, 139, 132–142,  
747 <https://doi.org/10.1016/j.dsr2.2016.09.006>, 2017.

748 Armstrong, R. A., Lee, C., Hedges, J. I., Honjo, S., and Wakeham, S. G.: A new, mechanistic model for  
749 organic carbon fluxes in the ocean based on the quantitative association of POC with ballast  
750 minerals, *Deep. Res. Part II Top. Stud. Oceanogr.*, 49, 219–236, [https://doi.org/10.1016/S0967-0645\(01\)00101-1](https://doi.org/10.1016/S0967-0645(01)00101-1), 2001.

752 Baumann, M., Joy Paul, A., Taucher, J., Thomas Bach, L., Goldenberg, S., Stange, P., Minutolo, F.,  
753 Riebesell, U., and Baumann mbaumann, M.: Drivers of Particle Sinking Velocities in the Peruvian  
754 Upwelling System, *EGU sphere. Prepr.*, 2022.

755 Belcher, A., Manno, C., Ward, P., Henson, S. A., Sanders, R., and Tarling, G. A.: Copepod faecal pellet  
756 transfer through the meso- and bathypelagic layers in the Southern Ocean in spring, *Biogeosciences*,  
757 14, <https://doi.org/10.5194/bg-14-1511-2017>, 2017.

758 Belcher, A., Manno, C., Thorpe, S., and Tarling, G.: Acantharian cysts: high flux occurrence in the  
759 bathypelagic zone of the Scotia Sea, Southern Ocean, *Mar. Biol.*, 165,  
760 <https://doi.org/10.1007/s00227-018-3376-1>, 2018.

761 Bidigare, R., Hanson, L., Buesseler, K. O., Wakeham, G., Freeman, H., Pancost, R. D., Millero, J.,  
762 Steinberg, P., Popp, N., Latasa, M., Landry, R., and Laws, A.: Iron-stimulated changes in  $^{13}\text{C}$   
763 fractionation and export by equatorial Pacific phytoplankton: Toward a paleogrowth rate proxy,  
764 *Paleoceanography*, 14, 589–595, <https://doi.org/10.1029/1999PA900026>, 1999.

765 Boehme, L., Meredith, M. P., Thorpe, S. E., Biuw, M., and Fedak, M.: Antarctic circumpolar current  
766 frontal system in the South Atlantic: Monitoring using merged Argo and animal-borne sensor data, *J.*  
767 *Geophys. Res.*, 113, C09012, <https://doi.org/10.1029/2007JC004647>, 2008.

768 Buesseler, K. O., Antia, A. N., Chen, M., Fowler, S. W., Gardner, W. D., Gustafsson, O., Harada, K.,  
769 Michaels, A. F., Rutgers van der Loeff, M., Sarin, M., Steinberg, D. K., and Trull, T.: An assessment of  
770 the use of sediment traps for estimating upper ocean particle fluxes, *J. Mar. Res.*, 65, 345–416,  
771 <https://doi.org/10.1357/002224007781567621>, 2007.

772 Cassar, N., Laws, E. A., Bidigare, R. R., and Popp, B. N.: Bicarbonate uptake by Southern Ocean  
773 phytoplankton, *Global Biogeochem. Cycles*, 18, 1–10, <https://doi.org/10.1029/2003GB002116>, 2004.



774 Cassarino, L., Hendry, K. R., Meredith, M. P., Venables, H. J., and De La Rocha, C. L.: Silicon isotope  
775 and silicic acid uptake in surface waters of Marguerite Bay, West Antarctic Peninsula, *Deep. Res. Part*  
776 *II Top. Stud. Oceanogr.*, 139, 143–150, <https://doi.org/10.1016/j.dsr2.2016.11.002>, 2017.

777 Cassarino, L., Hendry, K., Henley, S. F., Macdonald, E., Arndt, S., Freitas, F. S., Pike, J., and Firing, Y. L.:  
778 Sedimentary Nutrient Supply in Productive Hot Spots off the West Antarctic Peninsula Revealed by  
779 Silicon Isotopes, *Global Biogeochem. Cycles*, <https://doi.org/10.1029/2019GB006486>, 2020.

780 Checkley, D. M. and Entzeroth, L. C.: Elemental and isotopic fractionation of carbon and nitrogen by  
781 marine, planktonic copepods and implications to the marine nitrogen cycle, *J. Plankton Res.*, 7, 553–  
782 568, <https://doi.org/https://doi.org/10.1093/plankt/7.4.553>, 1985.

783 Closset, I., Cardinal, D., Bray, S. G., Thil, F., Djourae, I., Rigual-Hernández, A. S., and Trull, T. W.:  
784 Seasonal variations, origin, and fate of settling diatoms in the Southern Ocean tracked by silicon  
785 isotope records in deep sediment traps, *Global Biogeochem. Cycles*, 29, 1495–1510,  
786 <https://doi.org/10.1002/2015GB005180>, 2015.

787 Closset, I., Brzezinski, M. A., Cardinal, D., Dapoigny, A., Jones, J. L., and Robinson, R.: A silicon  
788 isotopic perspective on the contribution of diagenesis to the sedimentary silicon budget in the  
789 Southern Ocean, *Geochim. Cosmochim. Acta*, 327, 298–313, 2022.

790 Demarest, M. S., Brzezinski, M. A., and Beucher, C. P.: Fractionation of silicon isotopes during  
791 biogenic silica dissolution, *Geochim. Cosmochim. Acta*, 73, 5572–5583,  
792 <https://doi.org/10.1016/j.gca.2009.06.019>, 2009.

793 DeVries, T.: Atmospheric CO<sub>2</sub> and Sea Surface Temperature Variability Cannot Explain Recent  
794 Decadal Variability of the Ocean CO<sub>2</sub> Sink, *Geophys. Res. Lett.*, 49, 1–17,  
795 <https://doi.org/10.1029/2021GL096018>, 2022.

796 Egan, K. E., Rickaby, R. E. M., Leng, M. J., Hendry, K. R., Hermoso, M., Sloane, H. J., Bostock, H., and  
797 Halliday, A. N.: Diatom silicon isotopes as a proxy for silicic acid utilisation: A Southern Ocean core  
798 top calibration, *Geochim. Cosmochim. Acta*, 96, 174–192,  
799 <https://doi.org/10.1016/j.gca.2012.08.002>, 2012.

800 Ellwood, M. J., Strzpek, R. F., Strutton, P. G., Trull, T. W., Fourquez, M., and Boyd, P. W.: Distinct  
801 iron cycling in a Southern Ocean eddy, *Nat. Commun.*, 11, 1–8, [https://doi.org/10.1038/s41467-020-](https://doi.org/10.1038/s41467-020-14464-0)  
802 14464-0, 2020.

803 Fischer, G., Gersonde, R., and Wefer, G.: Organic carbon, biogenic silica and diatom fluxes in the  
804 marginal winter sea-ice zone and in the Polar Front Region: Interannual variations and differences in  
805 composition, *Deep. Res. Part II Top. Stud. Oceanogr.*, 49, 1721–1745,  
806 [https://doi.org/10.1016/S0967-0645\(02\)00009-7](https://doi.org/10.1016/S0967-0645(02)00009-7), 2002.

807 Friedrich, J. and Rutgers van der Loeff, M. M.: A two-tracer (<sup>210</sup>Po-<sup>234</sup>Th) approach to distinguish  
808 organic carbon and biogenic silica export flux in the Antarctic Circumpolar Current, *Deep. Res. Part I*  
809 *Oceanogr. Res. Pap.*, 49, 101–120, [https://doi.org/10.1016/S0967-0637\(01\)00045-0](https://doi.org/10.1016/S0967-0637(01)00045-0), 2002.

810 Georg, R. B., Reynolds, B. C., Frank, M., and Halliday, A. N.: New sample preparation techniques for  
811 the determination of Si isotopic compositions using MC-ICPMS, *Chem. Geol.*, 235, 95–104,  
812 <https://doi.org/10.1016/j.chemgeo.2006.06.006>, 2006.

813 Giering, S. L. C., Cavan, E. L., Basedow, S. L., Briggs, N., Burd, A. B., Darroch, L. J., Guidi, L., Irisson, J.  
814 O., Iversen, M. H., Kiko, R., Lindsay, D., Marcolin, C. R., McDonnell, A. M. P., Möller, K. O., Passow, U.,  
815 Thomalla, S., Trull, T. W., and Waite, A. M.: Sinking Organic Particles in the Ocean—Flux Estimates  
816 From in situ Optical Devices, *Front. Mar. Sci.*, 6, <https://doi.org/10.3389/fmars.2019.00834>, 2020.

817 Gleiber, M. R., Steinberg, D. K., and Ducklow, H. W.: Time series of vertical flux of zooplankton fecal

818 pellets on the continental shelf of the western Antarctic Peninsula, *Mar. Ecol. Prog. Ser.*, 471, 23–36,  
819 <https://doi.org/10.3354/meps10021>, 2012.

820 Glibert, P. M., Wilkerson, F. P., Dugdale, R. C., Raven, J. A., Dupont, C. L., Leavitt, P. R., Parker, A. E.,  
821 Burkholder, J. M., and Kana, T. M.: Pluses and minuses of ammonium and nitrate uptake and  
822 assimilation by phytoplankton and implications for productivity and community composition, with  
823 emphasis on nitrogen-enriched conditions, *Limnol. Oceanogr.*, 61, 165–197,  
824 <https://doi.org/10.1002/lno.10203>, 2016.

825 González, H. E., Daneri, G., Iriarte, J. L., Yannicelli, B., Menschel, E., Barría, C., Pantoja, S., and  
826 Lizárraga, L.: Carbon fluxes within the epipelagic zone of the Humboldt Current System off Chile: The  
827 significance of euphausiids and diatoms as key functional groups for the biological pump, *Prog.*  
828 *Oceanogr.*, 83, 217–227, <https://doi.org/10.1016/j.pocean.2009.07.036>, 2009.

829 Grasse, P., Brzezinski, M. A., Cardinal, D., De Souza, G. F., Andersson, P., Closset, I., Cao, Z., Dai, M.,  
830 Ehlert, C., Estrade, N., François, R., Frank, M., Jiang, G., Jones, J. L., Kooijman, E., Liu, Q., Lu, D.,  
831 Pahnke, K., Ponzevera, E., Schmitt, M., Sun, X., Sutton, J. N., Thil, F., Weis, D., Wetzels, F., Zhang, A.,  
832 Zhang, J., and Zhang, Z.: GEOTRACES inter-calibration of the stable silicon isotope composition of  
833 dissolved silicic acid in seawater, *J. Anal. At. Spectrom.*, 32, 562–578,  
834 <https://doi.org/10.1039/c6ja00302h>, 2017.

835 Grasse, P., Haynert, K., Doering, K., Geilert, S., Jones, J. L., Brzezinski, M. A., and Frank, M.: Controls  
836 on the Silicon Isotope Composition of Diatoms in the Peruvian Upwelling, *Front. Mar. Sci.*, 8, 1–15,  
837 <https://doi.org/10.3389/fmars.2021.697400>, 2021.

838 Grossart, H. P., Kjørboe, T., Tang, K., and Ploug, H.: Bacterial colonization of particles: Growth and  
839 interactions, *Appl. Environ. Microbiol.*, 69, 3500–3509, [https://doi.org/10.1128/AEM.69.6.3500-](https://doi.org/10.1128/AEM.69.6.3500-3509.2003)  
840 [3509.2003](https://doi.org/10.1128/AEM.69.6.3500-3509.2003), 2003.

841 Hansman, R. L. and Sessions, A. L.: Measuring the in situ carbon isotopic composition of distinct  
842 marine plankton populations sorted by flow cytometry, *Limnol. Oceanogr. Methods*, 14, 87–99,  
843 <https://doi.org/10.1002/lom3.10073>, 2016.

844 Hasle, G. R. and Syvertsen, E. E.: Chapter 2 – Marine Diatoms, in: *Identifying Marine Phytoplankton*,  
845 edited by: Tomas, C. R., Academic Press, San Diego, 5–385, 1997.

846 Hatton, J. E., Hendry, K. R., Hawkings, J. R., Wadham, J. L., Opfergelt, S., Kohler, T. J., Yde, J. C., Stibal,  
847 M., and Žárský, J. D.: Silicon isotopes in Arctic and sub-Arctic glacial meltwaters: The role of  
848 subglacial weathering in the silicon cycle, *Proc. R. Soc. A Math. Phys. Eng. Sci.*, 475,  
849 <https://doi.org/10.1098/rspa.2019.0098>, 2019.

850 Hawco, N. J., Barone, B., Church, M. J., Babcock-Adams, L., Repeta, D. J., Wear, E. K., Foreman, R. K.,  
851 Björkman, K. M., Bent, S., Van Mooy, B. A. S., Sheyn, U., DeLong, E. F., Acker, M., Kelly, R. L., Nelson,  
852 A., Ranieri, J., Clemente, T. M., Karl, D. M., and John, S. G.: Iron Depletion in the Deep Chlorophyll  
853 Maximum: Mesoscale Eddies as Natural Iron Fertilization Experiments, *Global Biogeochem. Cycles*,  
854 35, 1–18, <https://doi.org/10.1029/2021GB007112>, 2021.

855 Hendry, K. R. and Brzezinski, M. A.: Using silicon isotopes to understand the role of the Southern  
856 Ocean in modern and ancient biogeochemistry and climate, *Quat. Sci. Rev.*, 89, 13–26,  
857 <https://doi.org/10.1016/j.quascirev.2014.01.019>, 2014.

858 Hendry, K. R. and Robinson, L. F.: The relationship between silicon isotope fractionation in sponges  
859 and silicic acid concentration: Modern and core-top studies of biogenic opal, *Geochim. Cosmochim.*  
860 *Acta*, 81, 1–12, <https://doi.org/10.1016/j.gca.2011.12.010>, 2012.

861 Henley, S. F., Annett, A. L., Ganeshram, R. S., Carson, D. S., Weston, K., Crosta, X., Tait, A., Dougan,

862 J., Fallick, A. E., and Clarke, A.: Factors influencing the stable carbon isotopic composition of  
863 suspended and sinking organic matter in the coastal Antarctic sea ice environment, *Biogeosciences*,  
864 9, 1137–1157, <https://doi.org/10.5194/bg-9-1137-2012>, 2012.

865 Hillebrand, H., Dürselen, C. D., Kirschtel, D., Pollinger, U., and Zohary, T.: Biovolume calculation for  
866 pelagic and benthic microalgae, *J. Phycol.*, 35, 403–424, <https://doi.org/10.1046/j.1529-8817.1999.3520403.x>, 1999.

868 Honjo, S., Francois, R., Manganini, S., Dymond, J., and Collier, R.: Particle fluxes to the interior of the  
869 Southern Ocean in the Western Pacific sector along 170°W, *Deep. Res. Part II*, 47, 3521–3548,  
870 [https://doi.org/10.1016/S0967-0645\(00\)00077-1](https://doi.org/10.1016/S0967-0645(00)00077-1), 2000.

871 Iversen, M. H., Pakhomov, E. A., Hunt, B. P. V., Jagt, H. Van Der, Wolf-gladrow, D., and Klaas, C.:  
872 Sinkers or floaters? Contribution from salp pellets to the export flux during a large bloom event in  
873 the Southern Ocean, *Deep Sea Res. Part II Top. Stud. Oceanogr.*, 138, 116–125,  
874 <https://doi.org/10.1016/j.dsr2.2016.12.004>, 2017.

875 Kiørboe, T., Tang, K., Grossart, H. P., and Ploug, H.: Dynamics of microbial communities on marine  
876 snow aggregates: Colonization, growth, detachment, and grazing mortality of attached bacteria,  
877 *Appl. Environ. Microbiol.*, 69, 3036–3047, <https://doi.org/10.1128/AEM.69.6.3036-3047.2003>, 2003.

878 Korb, R. E., Whitehouse, M. J., Atkinson, A., and Thorpe, S.: Magnitude and maintenance of the  
879 phytoplankton bloom at South Georgia: a naturally iron-replete environment, *Mar. Ecol. Prog. Ser.*,  
880 368, 75–91, <https://doi.org/10.3354/meps07525>, 2008.

881 Korb, R. E., Whitehouse, M. J., Ward, P., Gordon, M., Venables, H. J., and Poulton, A. J.: Regional and  
882 seasonal differences in microplankton biomass, productivity, and structure across the Scotia Sea:  
883 Implications for the export of biogenic carbon, *Deep Sea Res. Part II Top. Stud. Oceanogr.*, 59–60,  
884 67–77, <https://doi.org/10.1016/j.dsr2.2011.06.006>, 2012.

885 Kwon, E., Primeau, F., and Sarmiento, J.: The impact of remineralization depth on the air-sea carbon  
886 balance, *Nat. Geosci.*, 2, 630–635, 2009.

887 De La Rocha, C. L., Brzezinski, M. A., and DeNiro, M. J.: Fractionation of silicon isotopes by marine  
888 diatoms during biogenic silica formation, *Geochim. Cosmochim. Acta*, 61, 5051–5056,  
889 [https://doi.org/10.1016/S0016-7037\(97\)00300-1](https://doi.org/10.1016/S0016-7037(97)00300-1), 1997.

890 Manno, C., Stowasser, G., Enderlein, P., Fielding, S., and Tarling, G. A.: The contribution of  
891 zooplankton faecal pellets to deep-carbon transport in the Scotia Sea (Southern Ocean),  
892 *Biogeosciences*, 12, 1955–1965, <https://doi.org/10.5194/bg-12-1955-2015>, 2015.

893 Manno, C., Fielding, S., Stowasser, G., Murphy, E. J., and Thorpe, S. E.: Continuous moulting by  
894 Antarctic krill drives major, *Nat. Commun.*, 16, 6051, <https://doi.org/10.1038/s41467-020-19956-7>,  
895 2020.

896 Matano, R. P., Combes, V., Young, E. F., and Meredith, M. P.: Modeling the Impact of Ocean  
897 Circulation on Chlorophyll Blooms Around South Georgia, *Southern Ocean, J. Geophys. Res. Ocean.*,  
898 125, 1–18, <https://doi.org/10.1029/2020JC016391>, 2020.

899 Medlin, L. K. and Priddle, J.: Polar marine diatoms, British Antarctic Survey, Cambridge, UK, 214 pp.,  
900 1990.

901 Meyerink, S. W., Boyd, P. W., Maher, W. A., Milne, A., Strzepek, R., and Ellwood, M. J.: Putting the  
902 silicon cycle in a bag: Field and mesocosm observations of silicon isotope fractionation in subtropical  
903 waters east of New Zealand, *Mar. Chem.*, 213, 1–12,  
904 <https://doi.org/10.1016/j.marchem.2019.04.008>, 2019.

- 905 Michener, R. and Lajtha, K.: *Stable Isotopes in Ecology and Environmental Science: Second Edition*,  
906 1–566 pp., <https://doi.org/10.1002/9780470691854>, 2008.
- 907 Minagawa, M. and Wada, E.: Stepwise enrichment of  $^{15}\text{N}$  along food chains: Further evidence and  
908 the relation between  $\delta^{15}\text{N}$  and animal age, *Geochim. Cosmochim. Acta*, 48, 1135–1140,  
909 [https://doi.org/10.1016/0016-7037\(84\)90204-7](https://doi.org/10.1016/0016-7037(84)90204-7), 1984.
- 910 Mincks, S. L., Smith, C. R., Jeffreys, R. M., and Sumida, P. Y. G.: Trophic structure on the West  
911 Antarctic Peninsula shelf: Detritivory and benthic inertia revealed by  $\delta^{13}\text{C}$  and  $\delta^{15}\text{N}$  analysis, *Deep.*  
912 *Res. Part II Top. Stud. Oceanogr.*, 55, 2502–2514, <https://doi.org/10.1016/j.dsr2.2008.06.009>, 2008.
- 913 Montoya, J. P.: Natural abundance of  $^{15}\text{N}$  in marine planktonic ecosystems, in: *Stable Isotopes in*  
914 *Ecology and Environmental Science: Second Edition*, edited by: Michener, R. and Lajtha, K., Blackwell  
915 Publishing, 1–566, <https://doi.org/10.1002/9780470691854>, 2007.
- 916 Moore, J. K., Abbott, M. R., and Richman, J. G.: Location and dynamics of the Antarctic Polar Front  
917 from satellite sea surface temperature data, *J. Geophys. Res. Ocean.*, 104, 3059–3073,  
918 <https://doi.org/10.1029/1998JC900032>, 1999.
- 919 Ng, H. C., Cassarino, L., Pickering, R. A., Woodward, E. M. S., Hammond, S. J., and Hendry, K. R.:  
920 Sediment efflux of silicon on the Greenland margin and implications for the marine silicon cycle,  
921 *Earth Planet. Sci. Lett.*, 529, 115877, <https://doi.org/10.1016/j.epsl.2019.115877>, 2020.
- 922 Nielsdóttir, M. C., Bibby, T. S., Moore, C. M., Hinz, D. J., Sanders, R., Whitehouse, M., Korb, R., and  
923 Achterberg, E. P.: Seasonal and spatial dynamics of iron availability in the Scotia Sea, *Mar. Chem.*,  
924 130–131, 62–72, <https://doi.org/10.1016/j.marchem.2011.12.004>, 2012.
- 925 Opfergelt, S. and Delmelle, P.: Silicon isotopes and continental weathering processes: Assessing  
926 controls on Si transfer to the ocean, *Comptes Rendus - Geosci.*, 344, 723–738,  
927 <https://doi.org/10.1016/j.crte.2012.09.006>, 2012.
- 928 Orsi, H., Whitworth III, T., and Nowlin Jr, W. D.: On the meridional extent and fronts of the Antarctic  
929 Circumpolar Current, *Deep Sea Res. Part I Oceanogr. Res. Pap.*, 42, 641–673,  
930 [https://doi.org/10.1016/0967-0637\(95\)00021-W](https://doi.org/10.1016/0967-0637(95)00021-W), 1995.
- 931 Passow, U. and De La Rocha, C. L.: Accumulation of mineral ballast on organic aggregates, *Global*  
932 *Biogeochem. Cycles*, 20, 1–7, <https://doi.org/10.1029/2005GB002579>, 2006.
- 933 Pauli, N.-C., Flintrop, C. M., Konrad, C., Pakhomov, E. A., Swoboda, S., Koch, F., Wang, X.-L., Zhang, J.-  
934 C., Brierley, A. S., Bernasconi, M., Meyer, B., and Iversen, M. H.: Krill and salp faecal pellets  
935 contribute equally to the carbon flux at the Antarctic Peninsula, *Nat. Commun.*, 12, 7168,  
936 <https://doi.org/10.1038/s41467-021-27436-9>, 2021.
- 937 Ploug, H., Iversen, M. H., and Fischer, G.: Ballast, sinking velocity, and apparent diffusivity within  
938 marine snow and zooplankton fecal pellets: Implications for substrate turnover by attached bacteria,  
939 *Limnol. Oceanogr.*, 53, 1878–1886, 2008.
- 940 Popp, B. N., Laws, E. A., Bidigare, R. R., Dore, J. E., Hanson, K. L., and Wakeham, S. G.: Effect of  
941 phytoplankton cell geometry on carbon isotopic fractionation, *Geochim. Cosmochim. Acta*, 62, 69–  
942 77, [https://doi.org/10.1016/S0016-7037\(97\)00333-5](https://doi.org/10.1016/S0016-7037(97)00333-5), 1998.
- 943 Popp, B. N., Trull, T., Kenig, F., Wakeham, S. G., Rust, T. M., Tilbrook, B., Griffiths, F. B., Wright, S. W.,  
944 Marchant, H. J., Bidigare, R. R., and Laws, E. A.: Controls on the carbon isotopic composition of  
945 Southern Ocean phytoplankton, *Global Biogeochem. Cycles*, 13, 827–843,  
946 <https://doi.org/10.1029/1999GB900041>, 1999.
- 947 Priddle, J. and Fryxell, G.: *Handbook of the common plankton diatoms of the Southern Ocean:*

- 948 Centrales except the genus *Thalassiosira*, British Antarctic Survey, Cambridge, UK, 159 pp., 1985.
- 949 Rau, G. H., Froelich, P. N., Takahashi, T., and J., D. M. D.: Does sedimentary organic  $\delta^{13}\text{C}$  record  
950 variations in quaternary ocean [ $\text{CO}_2(\text{aq})$ ], *Paleoceanography*, 6, 335–347, 1991.
- 951 Raven, J. A.: Inorganic Carbon Acquisition by Marine Autotrophs, *Adv. Bot. Res.*, 27, 85–209,  
952 [https://doi.org/10.1016/S0065-2296\(08\)60281-5](https://doi.org/10.1016/S0065-2296(08)60281-5), 1997.
- 953 Rembauville, M., Blain, S., Armand, L., Quéguiner, B., and Salter, I.: Export fluxes in a naturally iron-  
954 fertilized area of the Southern Ocean – Part 2: Importance of diatom resting spores and faecal  
955 pellets for export, *Biogeosciences*, 12, 3171–3195, <https://doi.org/10.5194/bg-12-3171-2015>, 2015.
- 956 Rembauville, M., Manno, C., Tarling, G. A., Blain, S., and Salter, I.: Strong contribution of diatom  
957 resting spores to deep-sea carbon transfer in naturally iron-fertilized waters downstream of South  
958 Georgia, *Deep. Res. Part I*, 115, 22–35, <https://doi.org/10.1016/j.dsr.2016.05.002>, 2016.
- 959 Reynolds, B. C., Aggarwal, J., André, L., Baxter, D., Beucher, C., Brzezinski, M. A., Engström, E., Georg,  
960 R. B., Land, M., Leng, M. J., Opfergelt, S., Rodushkin, I., Sloane, H. J., Van Den Boorn, S. H. J. M.,  
961 Vroon, P. Z., and Cardinal, D.: An inter-laboratory comparison of Si isotope reference materials, *J.*  
962 *Anal. At. Spectrom.*, 22, 561–568, <https://doi.org/10.1039/b616755a>, 2007.
- 963 Roberts, K., Granum, E., Leegood, R. C., and Raven, J. A.: Carbon acquisition by diatoms, *Photosynth.*  
964 *Res.*, 93, 79–88, <https://doi.org/10.1007/s1120-007-9172-2>, 2007.
- 965 Roca-Marti, M., Puigcorbé, V., Iversen, M. H., Rutgers van der Loeff, M., Klaas, C., Cheah, W.,  
966 Bracher, A., and Masqué, P.: High particulate organic carbon export during the decline of a vast  
967 diatom bloom in the Atlantic sector of the Southern Ocean, *Deep Sea Res. Part II Top. Stud.*  
968 *Oceanogr.*, 138, 102–115, <https://doi.org/10.1016/j.dsr2.2015.12.007>, 2017.
- 969 Salter, I., Kemp, A. E. S. S., Moore, C. M., Lampitt, R. S., Wolff, G. A., and Holtvoeth, J.: Diatom resting  
970 spore ecology drives enhanced carbon export from a naturally iron-fertilized bloom in the Southern  
971 Ocean, *Global Biogeochem. Cycles*, 26, 1–17, <https://doi.org/10.1029/2010GB003977>, 2012.
- 972 Sathyendranath, S., Brewin, R., Brockmann, C., Brotas, V., Calton, B., Chuprin, A., Cipollini, P., Couto,  
973 A., Dingle, J., Doerffer, R., Donlon, C., Dowell, M., Farman, A., Grant, M., Groom, S., Horseman, A.,  
974 Jackson, T., Krasemann, H., Lavender, S., Martinez-Vicente, V., Mazeran, C., Mélin, F., Moore, T.,  
975 Müller, D., Regner, P., Roy, S., Steele, C., Steinmetz, F., Swinton, J., Taberner, M., Thompson, A.,  
976 Valente, A., Zühlke, M., Brando, V., Feng, H., Feldman, G., Franz, B., Frouin, R., Gould, R., Hooker, S.,  
977 Kahru, M., Kratzer, S., Mitchell, B., Muller-Karger, F., Sosik, H., Voss, K., Werdell, J., and Platt, T.: An  
978 Ocean-Colour Time Series for Use in Climate Studies: The Experience of the Ocean-Colour Climate  
979 Change Initiative (OC-CCI), *Sensors*, 19, 4285, <https://doi.org/10.3390/s19194285>, 2019.
- 980 Sathyendranath, S., Jackson, T., Brockmann, C., Brotas, V., Calton, B., Chuprin, A., Clements, O.,  
981 Cipollini, P., Danne, O., Dingle, J., Donlon, C., Grant, M., Groom, S., Krasemann, H., Lavender, S.,  
982 Mazeran, C., Mélin, F., Müller, D., Steinmetz, F., Valente, A., Zühlke, M., Feldman, G., Franz, B.,  
983 Frouin, R., Werdell, J., and Platt, T.: ESA Ocean Colour Climate Change Initiative (Ocean\_Colour\_cci):  
984 Version 5.0 Data, NERC EDS Cent. Environ. Data Anal.,  
985 <https://doi.org/10.5285/1dbe7a109c0244aaad713e078fd3059a>, 2021.
- 986 Schmidt, K., Atkinson, A., Stübing, D., McClelland, J. W., Montoya, J. P., and Voss, M.: Trophic  
987 relationships among Southern Ocean copepods and krill: Some uses and limitations of a stable  
988 isotope approach, *Limnol. Oceanogr.*, 48, 277–289, <https://doi.org/10.4319/lo.2003.48.1.0277>,  
989 2003.
- 990 Scott, F. J. and Marchant, H. J. (Eds.): *Antarctic Marine Protists*, Australian Biological Resources  
991 Study, Canberra, 2005.

- 992 Shen, C., Dupont, C. L., and Hopkinson, B. M.: The diversity of CO<sub>2</sub>-concentrating mechanisms in  
 993 marine diatoms as inferred from their genetic content, *J. Exp. Bot.*, 68, 3937–3948,  
 994 <https://doi.org/10.1093/jxb/erx163>, 2017.
- 995 Sigman, D. M. and Fripiat, F.: Nitrogen isotopes in the ocean, *Encycl. Ocean Sci.*, 263–278,  
 996 <https://doi.org/10.1016/B978-0-12-409548-9.11605-7>, 2019.
- 997 Smetacek, V., Assmy, P., and Henjes, J.: The role of grazing in structuring Southern Ocean pelagic  
 998 ecosystems and biogeochemical cycles, *Antarct. Sci.*, 16, 541–558,  
 999 <https://doi.org/10.1017/S0954102004002317>, 2004.
- 1000 Strickland, J. and Parsons, T.: *A Practical Handbook of Seawater Analysis*, Fisheries Research Board of  
 1001 Canada, 405 pp., <https://doi.org/10.2307/1979241>, 1972.
- 1002 Sutton, J. N., Varela, D. E., Brzezinski, M. A., and Beucher, C. P.: Species-dependent silicon isotope  
 1003 fractionation by marine diatoms, *Geochim. Cosmochim. Acta*, 104, 300–309,  
 1004 <https://doi.org/10.1016/j.gca.2012.10.057>, 2013.
- 1005 Tamelander, T., Søreide, J. E., Hop, H., and Carroll, M. L.: Fractionation of stable isotopes in the Arctic  
 1006 marine copepod *Calanus glacialis*: Effects on the isotopic composition of marine particulate organic  
 1007 matter, *J. Exp. Mar. Bio. Ecol.*, 333, 231–240, <https://doi.org/10.1016/j.jembe.2006.01.001>, 2006.
- 1008 Thorpe, S. E., Heywood, K. J., Brandon, M. A., and Stevens, D. P.: Variability of the southern Antarctic  
 1009 Circumpolar Current front north of South Georgia, *J. Mar. Syst.*, 37, 87–105,  
 1010 [https://doi.org/10.1016/S0924-7963\(02\)00197-5](https://doi.org/10.1016/S0924-7963(02)00197-5), 2002.
- 1011 Torres Valdés, S., Painter, S. C., Martin, A. P., Sanders, R., and Felden, J.: Data compilation of fluxes  
 1012 of sedimenting material from sediment traps in the Atlantic ocean, *Earth Syst. Sci. Data*, 6, 123–145,  
 1013 <https://doi.org/10.5194/essd-6-123-2014>, 2014.
- 1014 Trimborn, S., Wolf-Gladrow, D., Richter, K. U., and Rost, B.: The effect of pCO<sub>2</sub> on carbon acquisition  
 1015 and intracellular assimilation in four marine diatoms, *J. Exp. Mar. Bio. Ecol.*, 376, 26–36,  
 1016 <https://doi.org/10.1016/j.jembe.2009.05.017>, 2009.
- 1017 Trull, T. W. and Armand, L.: Insights into Southern Ocean carbon export from the  $\delta^{13}\text{C}$  of particles  
 1018 and dissolved inorganic carbon during the SOIREE iron release experiment, *Deep. Res. Part II Top.*  
 1019 *Stud. Oceanogr.*, 48, 2655–2680, [https://doi.org/10.1016/S0967-0645\(01\)00013-3](https://doi.org/10.1016/S0967-0645(01)00013-3), 2001.
- 1020 Tuerena, R. E., Ganeshram, R. S., Humphreys, M. P., Browning, T. J., Bouman, H., and Piotrowski, A.  
 1021 P.: Isotopic fractionation of carbon during uptake by phytoplankton across the South Atlantic  
 1022 subtropical convergence, *Biogeosciences*, 16, 3621–3635, <https://doi.org/10.5194/bg-16-3621-2019>,  
 1023 2019.
- 1024 Volk, T. and Hoffert, M. I.: Ocean Carbon Pumps: Analysis of relative strengths and efficiencies in  
 1025 ocean driven atmospheric CO<sub>2</sub> changes, in: *The carbon cycle and atmospheric CO<sub>2</sub>: Natural variations*  
 1026 *Archean to Present*, edited by: Sundquist, E. T. and Broecker, W. S., American Geophysical Union,  
 1027 Washington, DC, 99–110, 1985.
- 1028 Wada, E. and Hattori, A.: Nitrogen isotope effects in the assimilation of inorganic nitrogenous  
 1029 compounds by marine diatoms, *Geomicrobiol. J.*, 1, 85–101,  
 1030 <https://doi.org/10.1080/01490457809377725>, 1978.
- 1031 Wada, E., Terazaki, M., Kabaya, Y., and Nemoto, T.: <sup>15</sup>N and <sup>13</sup>C abundances in the Antarctic Ocean  
 1032 with emphasis on the biogeochemical structure of the food web, *Deep Sea Res. Part A, Oceanogr.*  
 1033 *Res. Pap.*, 34, 829–841, [https://doi.org/10.1016/0198-0149\(87\)90039-2](https://doi.org/10.1016/0198-0149(87)90039-2), 1987.
- 1034 Ward, J. P. J., Hendry, K. R., Arndt, S., Faust, J. C., Freitas, F. S., Henley, S. F., Krause, J. W., März, C.,

- 1035 Ng, H. C., Pickering, R. A., and Tessin, A. C.: Stable silicon isotopes uncover a mineralogical control on  
1036 the benthic silicon cycle in the Arctic Barents Sea, *Geochim. Cosmochim. Acta*, 329, 206–230,  
1037 <https://doi.org/10.1016/j.gca.2022.05.005>, 2022.
- 1038 Weir, I., Fawcett, S., Smith, S., Walker, D., Bornman, T., and Fietz, S.: Winter biogenic silica and  
1039 diatom distributions in the Indian sector of the Southern Ocean, *Deep. Res. Part I Oceanogr. Res.*  
1040 *Pap.*, 166, 103421, <https://doi.org/10.1016/j.dsr.2020.103421>, 2020.
- 1041 Wetzel, F., de Souza, G. F., and Reynolds, B. C.: What controls silicon isotope fractionation during  
1042 dissolution of diatom opal?, *Geochim. Cosmochim. Acta*, 131, 128–137,  
1043 <https://doi.org/10.1016/j.gca.2014.01.028>, 2014.
- 1044 White, W. M., Albarède, F., and Télouk, P.: High-precision analysis of Pb isotope ratios by multi-  
1045 collector ICP-MS, *Chem. Geol.*, 167, 257–270, [https://doi.org/10.1016/S0009-2541\(99\)00182-5](https://doi.org/10.1016/S0009-2541(99)00182-5),  
1046 2000.
- 1047 Whitehouse, M. J., Priddle, J., Trathan, P. N., and Brandon, M. A.: Substantial open-ocean  
1048 phytoplankton blooms to the north of South Georgia, South Atlantic, during summer 1994, *Mar.*  
1049 *Ecol. Prog. Ser.*, 140, 187–197, <https://doi.org/10.3354/meps140187>, 1996.
- 1050 Young, J. N., Heureux, A. M. C., Sharwood, R. E., Rickaby, R. E. M., Morel, F. M. M., and Whitney, S.  
1051 M.: Large variation in the Rubisco kinetics of diatoms reveals diversity among their carbon-  
1052 concentrating mechanisms, *J. Exp. Bot.*, 67, 3445–3456, <https://doi.org/10.1093/jxb/erw163>, 2016.
- 1053